Citation: Šarinová, K., Rybár, S., Jourdan, F., Frew, A., Mayers, C., Kováčová, M., Lichtman, B., Nováková, P., Kováč, M., 2021. $^{40}Ar/^{39}Ar$ geochronology of Burdigalian paleobotanical localities in the central Paratethys (south Slovakia). Geologica Acta, Vol.19.5, 1-19, I-IV.
DOI: 10.1344/GeologicaActa2021.19.5

geologica acta

$^{40}Ar/^{39}Ar$ geochronology of Burdigalian paleobotanical localities in the central Paratethys (South Slovakia)

Katarína Šarinová[1] Samuel Rybár [2,3] Fred Jourdan [4,5] Adam Frew[4] Celia Mayers[4] Marianna Kováčová[2] Barbara Lichtman[1] Petronela Nováková[2] Michal Kováč[2]

[1]Department of mineralogy and petrology, Faculty of Natural Sciences, Comenius University
Mlynská dolina, Ilkovičova 6, 842 15 Bratislava, Slovakia. Šarinová E-mail: katarina.sarinova@uniba.sk

[2]Department of geology and paleontology, Faculty of Natural Sciences, Comenius University
Mlynská dolina, Ilkovičova 6, 842 15 Bratislava, Slovakia

[3]Energy & Geoscience Inst. at University of Utah
423 Wakara Way, Suite 300, Salt Lake City, UT 84108, USA

[4]Western Australian Argon Isotope Facility and John de Laeter Centre, Curtin University
Perth, Western Australia 6845, Australia

[5]School of Earth and Planetary, SSTC and TIGeR, Curtin University
Perth, Western Australia 6845, Australia

ABSTRACT

The Lipovany and Mučín paleobotanical localities contain important floral associations within the tuff horizons, which were used for determination of subtropical to tropical climatic conditions during the Early Miocene. Based on the combination of results from plagioclase and biotite $^{40}Ar/^{39}Ar$ dating, the age of the tuff deposition is around 17.3Ma. For the Lipovany locality, single-grain $^{40}Ar/^{39}Ar$ convergent ages of 17.49±0.54Ma and 17.28±0.06Ma, for plagioclase and biotite were obtained, respectively. The Mučín locality only provide an imprecise convergent age of 16.5±1.4Ma due to the small size of the analyzed plagioclase crystals. The results thus allowed to include the fossil subtropical flora of the studied localities in the late Ottnangian regional stage (upper part of the Burdigalian). Additionally, these age data indicate that deposition of the overlaying Salgótarján Formation starts much later than originally thought (during Ottnangian-Karpatian boundary).

KEYWORDS **Ottnangian; Gyulakeszi Rhyolite Tuff Formation; $^{40}Ar/^{39}Ar$ Dating; Petrography; Sedimentology.**

INTRODUCTION

The studied paleontological sites Lipovany and Mučín crop out in the Cerová vrchovina Highland near the Slovak-Hungarian state border (Fig. 1). Since the spatial distribution of the studied tuffs includes both, the Slovak and Hungarian territory, stratigraphic unit names will be given both in Slovak and Hungarian.

The fossiliferous tuff and ignimbrite from the Lipovany and Mučín sections belong to the same volcanic formation as the Hungarian Ipolytarnóc section (*e.g.* Erdei *et al.,*

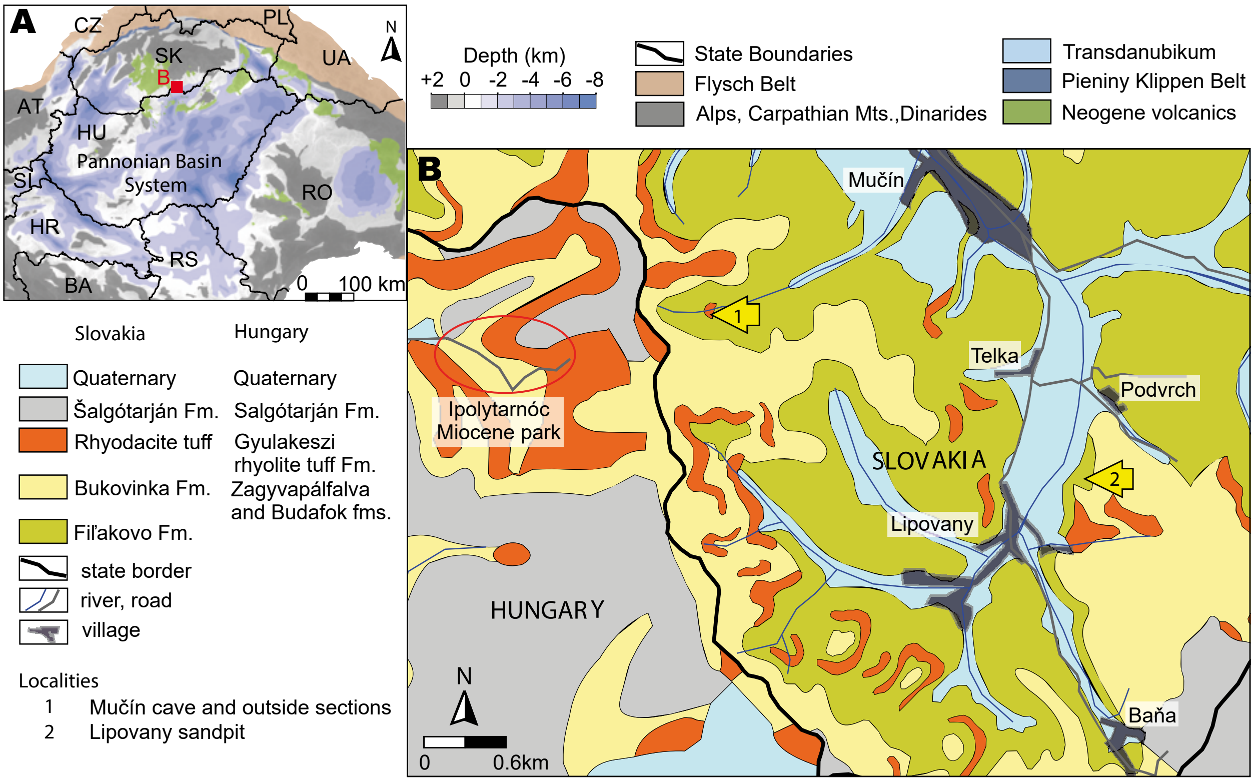

FIGURE 1. A) Location of the study area (B) in the Alpine–Carpathian–Pannonian system (compiled from Fusán *et al.*, 1987; Hók *et al.*, 2014; Horváth *et al.*, 2015; Nováková *et al.*, 2020). B) Geologic map of the study area showing location of studied sections (compiled by Gyalog and Síkhegyi, 2005 and by Vass, 1992). SK: Slovakia, CZ: Czechia, PL: Poland, UA: Ukraine, AT: Austria, HU: Hungary, SI: Slovenia, HR: Croatia, RO: Romania, RS: Serbia, BA: Bosnia and Herzegovina.

2007; Hably, 1985; Márton *et al.*, 2007; Pálfy *et al.*, 2007; Sitár and Kvaček, 1997; Vass *et al.*, 2006). The area in the vicinity of Lipovany-Mučín-Ipolytarnóc belongs to the Ipolytarnoc Fossils Nature Conservation Area (Fig. 1). These three localities include rich fossil plant assemblages consisting of about 41 genera and 65 species of leaf remains (*e.g.* Hably, 1985; Kučerová, 2009; Němejc and Knobloch, 1969; Sitár and Kvaček, 1997). The importance of the mentioned localities follows from the very good preservation of leaf impressions that enabled interpretation of morphological characteristics and from the numerous remains sufficient for statistical evaluation (Hably, 1985). Mentioned localities also contain silicified tree trunks (*e.g.* Hably, 1985; Sitár and Kvaček, 1997) and Ipolytarnóc locality contains mammal and bird footprints localized immediately under the tuff (see Kordos, 1985). The assemblage of taxa is dominated by laurophyllous plants, indicative of a subtropical rainforest developed in a warm and humid climate (*e.g.* Hably, 1985; Kučerová, 2009; Sitár and Kvaček, 1997). Vegetation from the Lipovany section was last described as a multi storeyed forest with higher canopy occupied by *Platanus neptuni, Engelhardia* and admixture of *Pinus*; lower tree storey with Lauraceae, *Tetraclinis, Magnolia, Cyclocarya* and *Cassia*; and the shrub storey with palms, Lauraceae, enigmatic *Pungiphyllum*, Theaceae and "*Celastrus*" (Sitár and Kvaček, 1997). From the taphonomic point of view, almost no cuticles were preserved due to fusinisation. The Mučín locality was last studied by Kučerová (2009), who documented dominance of *Celastrus* genus supplemented by *Platanus neptuni*, *Engelhardia orsbergensis*, *Cassia berenices*, *Podocarpium podocarpum*, *Dalbergia nostratum* and *Leguminosites* sp.

The flora from the Lipovany section was previously described as parastratotype for the Ottnangian regional stage (Němejc and Knobloch, 1973). The first dating of the tuffs using the Fission Track method (FT; biotite) indicated an age of 20.1±0.3Ma (Repčok, 1987), thus it was considered Eggenburgian (lower Burdigalian) in age (Vass, 2002; Vass *et al.*, 2006). Additionally, similar and rather imprecise K/Ar radioisotopic ages of 20.0±2.0Ma (biotite) and 19.8±3.0Ma (plagioclase; Hámor *et al.*, 1979 in Pálfy *et al.*, 2007) were obtained from the neighboring Ipolytarnóc area. However, subsequent paleomagnetic results (Márton, 2007; Márton *et al.*, 2007; Vass *et al.*, 2006) suggested, that the ignimbrite together with footprints containing sandstone from the Ipolytarnóc area are younger than expected. Finally, a younger date was supplemented by new radioisotopic age of 17.42±0.04Ma by U-Th and 17.02±0.14Ma by $^{40}Ar/^{39}Ar$ (Pálfy *et al.*, 2007). This $^{40}Ar/^{39}Ar$ date was recalculated to

TABLE 1. Table of all the available ages calculated using the constants of Renne *et al.* (2011)

locality	original data $^{40}Ar/^{39}Ar$ data	calculated using the constants of Renne *et al.* (2011)
Ipolytarnóc (GRTF; known as Fehérhegy Fm.), Hungary	17.02 ± 0.14 Ma; (Pálfy *et al.*, 2007)	17.19 ± 0.14 Ma; plagioclase
Lipovany (GRTF; known as Fehérhegy Fm.), Slovakia		17.49 ± 0.54 Ma; plagioclase 17.28 ± 0.06 Ma; biotite
Mučín (GRTF; known as Fehérhegy Fm.); Slovakia		16.5 ± 1.4 Ma; plagioclase
Straning tuff; Austria	17.23 ± 0.18 Ma; (Roetzel *et al.*, 2014)	17.29 ± 0.18 Ma; K-feldspar

17.19±0.14Ma using the constants of Renne *et al.* (2011; Table 1) which are fully calibrated against the U-Pb system (Renne *et al.*, 2010). These data shift the studied ignimbrites toward the Ottnangian/Karpatian boundary (ca. to mid/upper part of the Burdigalian stage). However, magnetostratigraphy of the fosilliferous Lipovany section (NE Lipovany) revealed a reverse polarity opposite to normal polarity in the Mučín and Ipolytarnóc sections (Vass *et al.*, 2006; Márton *et al.*, 2007). Therefore, the mentioned authors erroneously decided to leave the Lipovany section assigned to the Eggenburgian.

The main aim of this paper is to present new $^{40}Ar/^{39}Ar$ radioisotopic data from key paleobotanical Lipovany and Mučín sections. The new data will also contribute to the lithostratigraphic and paleogeographic framework of the area, as well as to the paleovegetation and paleoclimate evolution model.

GEOLOGICAL SETTING

The oldest outcropping sediments in the study area consists of marine sandstones with some tuffs intercalations, and belong to the Lipovany Member (Mb.) of the Fiľakovo Formation (Fm.)/Pétervására or Budafolk Fm. (Fig. 1; 2A) (Bartkó, 1985; Pálfy *et al.*, 2007; Vass and Elečko, 1992; Vass, 2002). The depositional environment of the sandstones has been interpreted as a nearshore or coastal to intertidal dominated by tidal flows. An erosive surface characterizes the boundary between the Lipovany/Pétervására sandstone and the overlaying terrestrial clastics of the Bukovinka/Zagyvapálfalva Fm. (Bartkó, 1985; Pálfy *et al.*, 2007; Vass and Elečko, 1992; Vass, 2002; Vass *et al.*, 2006). The Bukovinka/Zagyvapálfalva Fm. consits of fluvial sandstones and conglomerates along with variegated mudstones. In the Hungarian part, mammalian footprints have been described in these sandstones (see Kordos, 1985). The sandstone beds rich in mammal tracks were named Ipolytarnóc beds (Bartkó, 1985). The Bukovinka/Zagyvapálfalva Fm. is covered by the studied pyroclastic rocks. These tuffs and three ignimbrite sheets were traditionally ranked to "lower rhyolite tuffs" or to the Gyulakeszi Rhyolite Tuff Formation (GRTF) in Hungary (*e.g.* Vass, 2002; Lukács *et al.*, 2018; Pálfy *et al.*, 2007). In Slovakia they were originally part of the Bukovinka Fm. (*e.g.* Vass, 2002). Nonetheless, based on paleomagnetic data, these ignimbrites were withdrawn from the GRTF and incorporated to the newly defined Fehérhegy Fm. (Vass *et al.*, 2006; Márton *et al.*, 2007). During the age revision of the Bükkalja Volcanic Field the Ipolytarnóc ignimbrites were correlated with the Eger and Mangó units with an age range of 17.5 to 17.1Ma (Lukács *et al.*, 2018). More recent papers correlated deposition of these tuffs with the Salgótarján Fm. (Fig. 2A; Vass *et al.*, 2006; Márton *et al.*, 2007), which is composed of fluvial and lagoonal sandstones to claystones with coal intervals (Bartkó, 1985; Vass, 2002). Beyond the study area, the Salgótarján Fm. is covered by shallow marine calcareous mudstones to sandstones of the Modrý Kameň Fm./Gar*á*b Schlier Fm. and the Egyházasgerge Sandstone Fm. (Bartkó, 1985; Vass and Elečko, 1992; Vass, 2002).

The age of the described formations was determined based on biostratigraphy and original radiometric data. The marine Lipovany sandstone Mb. of the Fiľakovo Fm./Pétervására Sandstone Fm. was assigned to the Eggenburgian (Bartkó, 1985; Vass and Elečko eds., 1992; Vass, 2002), on the basis of identification of the NN3 nannoplakton zone (Holcová, 2001; Nagymarosy and Müller, 1988). The $^{87}Sr/^{86}Sr$ data from mollusk shells of the Lipovany Mb. provided an age range between 19.45 and 18.6Ma (Vass *et al.*, 2003). These ages were younger than the original FT age inferred by Repčok (1987; 20.6Ma). Additionally, the same age of 18.6±0.6Ma was estimated by using $^{87}Sr/^{86}Sr$ extracted from shark teeth from the Pétervására Fm. in Ipolytarnóc (Kocsis *et al.*, 2009). In the Salgótarján Fm. the NN3-NN4 nannoplankton zone was described (Holcová, 2001; Vass *et al.*, 1987). The shallow marine Modrý Kameň Fm./Garáb Schlier and Egyházasgerge Sandstone formations are assigned to the

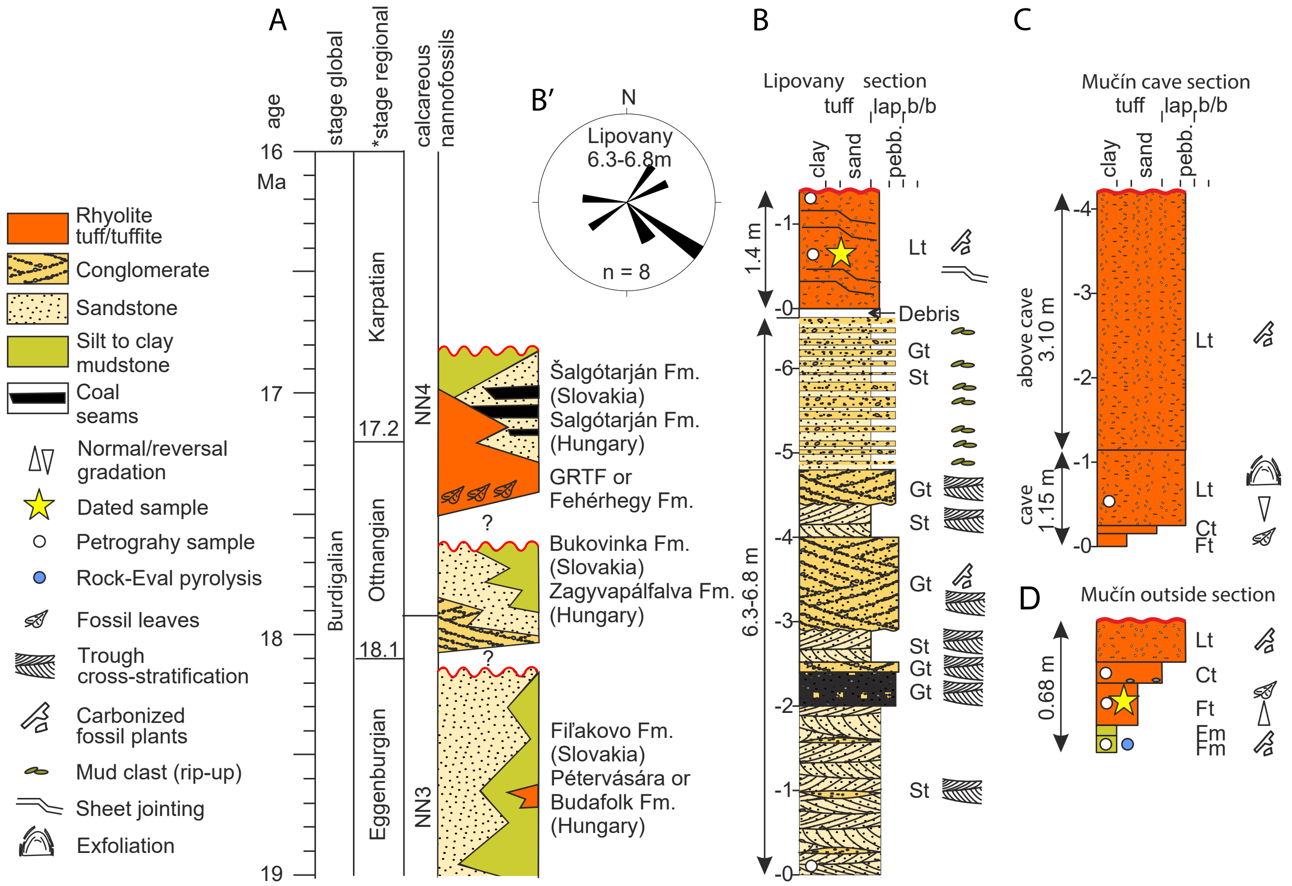

E Lithofacies code	Lithofacies	Sedimentary textures	Depositional processes, interpretations
Gt	Gravel, stratified	Trough cross-stratification, rip-up clasts	Channel fills, traction transport
St	Sand, may be pebbly	Trough cross-stratification	Sinuous-crested and linguoid dunes (3D), traction
Fm	Silt, clay	Massive	Ephemeral lake, aluvial plain, suspension
Lt	Lapilli tuff	Massive, occasional reverse gradation	Pyroclastic flow
Ct	Coarse tuff/sand	Massive	Pyroclastic surge or wash
Ft	Fine tuff	Massive, occasional normal gradation	Pyroclastic fall-deposits

FIGURE 2. A) Stratigraphic framwork of the study area (global stage and nannoplankton zonation adopted from TimeScale Creator GT, 2016; *regional stages adopted from Harzhauser *et al.*, 2019), B) Lipovany section log, B') Lipovany cross-stratification dipp Gt-St, C) Mučín cave section log, D) Mučín outside section log, E) Lithofacies code table.

Karpatian (Bartkó, 1985; Holcová, 2001; Vass and Elečko, 1992; Vass, 2002), but a new study correlates the Modrý Kameň Fm. with the upper part of NN4 zone (Ruman *et al.*, 2021). New ranking of the formations is presented in Figure 2. However, in the Mu*čín and Lipovany* area, the sedimentary sequences ended by the dated ignimbrites or by Salgótarján Fm. (Bartkó, 1985; Vass and Elečko, 1992).

METHODOLOGY

Sedimentology and petrography

The outcrops were manually excavated to expose the section, located in old quarries and in forest scours, and cleaned by palette knifes and brushes. The lithofacies abbreviations were adopted and modified from Németh and Martin (2007) and Miall (2006).

The mineralogy of specified lithotypes were studied under polarizing microscope. Samples from the fine grained tuff and lapilli tuff were analyzed under the Cameca SX 100 microprobe (State Geological Institute of Dionýz Štúr). Minerals were identified using WDS analysis with accelerating voltage 15keV, probe current 20nA, with a beam width of 10µm. These conditions were also used for some glass shards. Second group of vitroclasts were analysed under 2 conditions: probe current 3nA (Na, K, Si) and 10nA (other elements) for elimination of mobile element loss. Raw analyses were recalculated to weight percent of oxide using the ZAF correction. Other minerals were determined by EDAX analyses.

Six whole rocks samples plus one reference sample from Ipolytarnóc were crushed and send to Bureau Veritas mineral laboratories (Canada, Vancouver). Samples were pulverized and processed by Lithium Borate Fusion. Major elements were analyzed by ICP-ES, and trace elements by ICP-MS. One sample from the Mučín mudstones was selected for Rock-Eval pyrolysis (done in Montanuniversität Leoben).

$^{40}Ar/^{39}Ar$ dating method

Two whole rock tuff samples from Lipovany and Mučín sections (GRTF, Fig. 2) were sent to Western Australian Argon Isotope Facility of Curtin University for separation of minerals (plagioclase, biotite) and $^{40}Ar/^{39}Ar$ dating.

Plagioclase and biotite crystals were separated from 150-215µm and 215-315µm fractions using a Frantz isodynamic magnetic separator and then hand-picked grain-by-grain under a binocular stereomicroscope. Plagioclase crystals were further leached using diluted HF (2N) for 5 minutes and thoroughly rinsed in distilled water to remove any adhering alteration.

The samples were loaded into two 1.9cm-diameter and 0.3cm-depth Al disks that contain multiple smaller sample wells; all sample wells containing the separated crystals were surrounded by sample wells that carried the Fish Canyon sanidine neutron fluence monitor (28.294 [±0.13%]Ma; Jourdan and Renne, 2007; Renne *et al.,* 2011). The sample disks were Cd-shielded (to minimize undesirable nuclear interference reactions) and irradiated for 40h in the TRIGA reactor (Oregon State University, USA), in a central position. The J-value and mass discrimination factor are given in Annex 1. The correction factors for interfering isotopes were $(^{39}Ar/^{37}Ar)_{Ca} = 6.95 \cdot 10^{-4}$ (±1.3%), $(^{36}Ar/^{37}Ar)_{Ca} = 2.65 \cdot 10^{-4}$ (± 0.83%) measured on CaF_2 and $(^{40}Ar/^{39}Ar)_K = 7.02 \cdot 10^{-4}$ (± 12%) determined on K-Fe glass (Renne *et al.,* 2013). Ar isotopic data are corrected for blank, mass discrimination, and radioactive decay. Individual uncertainties are reported in Appendix I at the 1σ level unless otherwise indicated.

For each sample, a series of single crystals were fused in a single step using a continuous 100 W PhotonMachine© CO2 (IR, 10.6μm) laser fired on the aliquot material for 60 seconds. All standard crystals were fused in a single step. The gas was purified in an extra low-volume stainless steel extraction line of 240cm^3, set up to run with two SAES AP10 and one GP50 getter. Ar isotopes were measured in static mode using a low-volume (600cm^3) ARGUS VI mass spectrometer from Thermo Fisher© set with a permanent resolution of ~200. Measurements were carried out in multi-collection mode using three Faraday cups equipped with three 10^{12} ohm (masses 40; 38; and 37) and one 10^{13}ohm (mass 39) resistor amplifiers and a low background Compact Discrete Dynode (CDD) ion counter to measure mass 36. We measured the relative abundance of each mass simultaneously during 10 cycles of peak-hopping and 16 seconds of integration time for each mass. Detectors were calibrated to each other through air shot beam signals. Blanks were analyzed for every three to four incremental heating steps and typical ^{40}Ar blanks range from $1 \cdot 10^{-16}$ to $2 \cdot 10^{-16}$ mol. Mass discrimination was monitored using an automatic air pipette and values are provided in Appendix I in per Dalton (atomic mass unit).

Criteria for the determination of a convergent age are as follows: an age must include at least 3 consecutive single crystal ages agreeing at 95% confidence level and satisfying a probability of fit (P) of at least 0.05. Convergent ages are given at the 2σ level and are calculated using the mean of all the plateau steps, each weighted by the inverse variance of their individual analytical error. The raw data (Appendix I) were processed using the ArArCALC software (Koppers, 2002), and the ages have been calculated using the decay constants recommended by Renne *et al.* (2011). All analytical parameters and relative abundance values are provided in Table 1 and Appendix I and have been corrected for blanks, mass discrimination and radioactive decay. Individual errors in Appendix I are given at the 1σ level. Convergent ages include uncertainties on the decay constants and standard age, and were calculated using the Monte Carlo approach of Renne *et al.* (2010).

RESULTS

Facies analysis

Mučín three mould cave locality (GPS: N 48.23322º, E 19.67651º) is an outcrop accessible by a forest trail from the Mučín village (Fig. 1). The sections are exposed in a creek valley and bounded by a forest scour. Outcrop includes a small cave enclosed within the basal part of a lapilli tuff and a minor section outside the cave, approximately 20-25m before the cave entrance (Fig. 3). Several layers can be described in both partial sections (Fig. 2B; 3C-D). In the lowermost part of both sections, dark mudstones (Fm.; for lithofacies explanation see Figure 2) are present. At the outside section a 4cm thick brown clay (Fm.; Fig. 2D) is present above the dark mudstone. Higher up in both sections, fine grained tuff (Ft) with some gradation follow. Thickness of the fine tuff is between 14cm in the cave and 21cm outside the cave. The maximum grain-size of clasts is circa 1mm; samples show moderate sorting with recognizable normal gradation. The sample for $^{40}Ar/^{39}Ar$ dating was taken from the fine tuff of the outside section (Fig. 2D; 3E, H). The fine tuff is overlain by 10cm of coarse-grained tuff(Ct) with well-rounded sandstone extraclasts

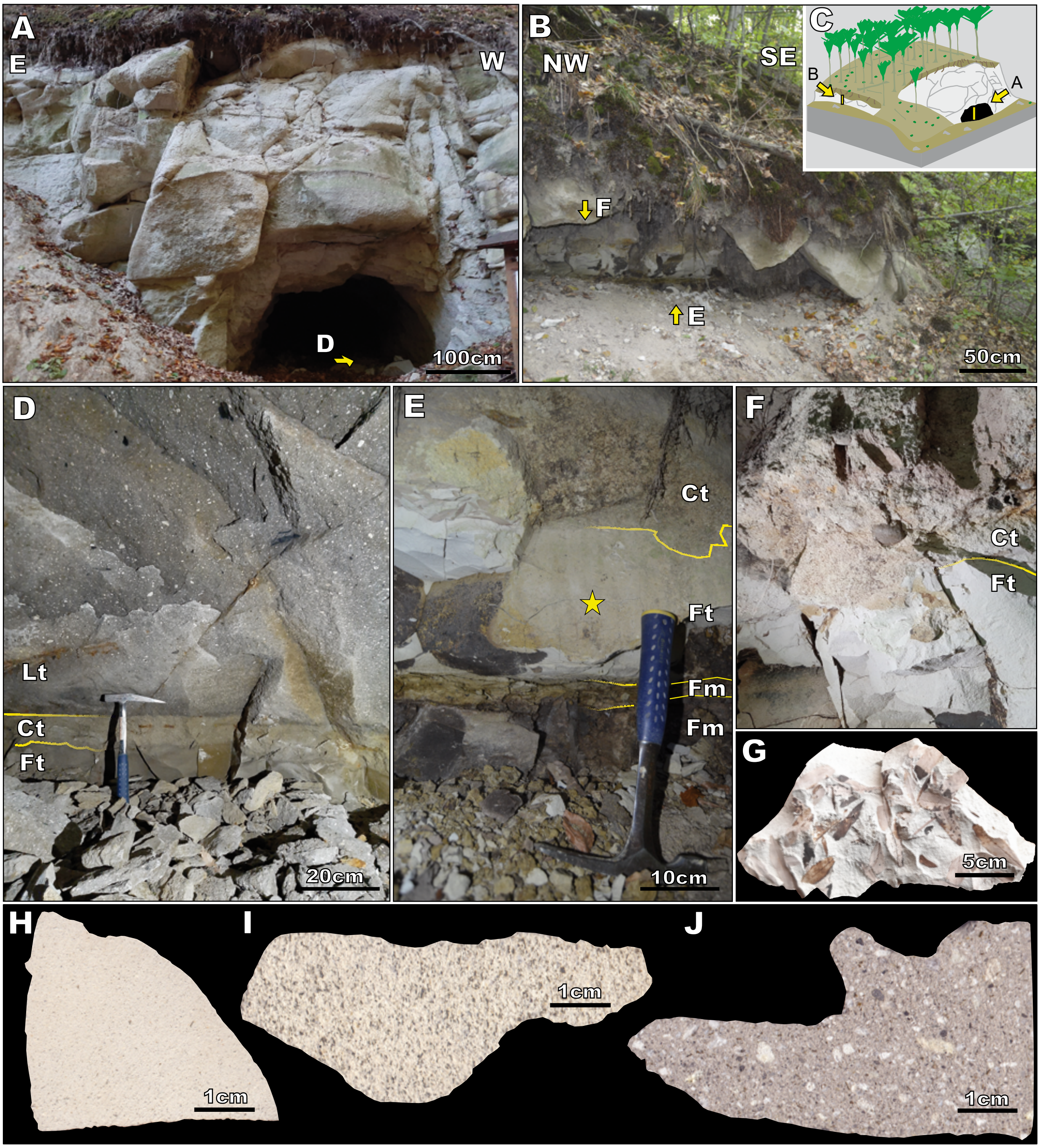

FIGURE 3. Mučín cave section: A) Mučika cave. B) Mučín outside section. C) Sketch with position of the Mučín localities. D) Detail of cave section with observable reverse gradation in the lapilli tuff (Lt). E) Detail of outside section with $^{40}Ar/^{39}Ar$ sample position marked by star. F) Pebbles inside sandy layer. G) Fossil leaves from the boundary between the fine tuff and sandy layer. H) Dated fine grained tuff. I) Sandy tuff or volcanic sandstone. J) Lapilli tuff. For abbreviation see Figure 2.

(ca. 3cm) at the base (Fig. 3E). The coarse-grained tuff is well sorted and dominantly formed of 2mm large clasts. Especially biotite shows preferential orientation of clasts (Fig. 3I). The top of the sections are characterized by a lapilli tuff layer (Lt) and a recent soil layer. The lapilli tuff layer shows no sorting but inverse gradation (Fig. 3C). It contains a high amount of approximately 10mm large pumice fragments and carbonized plant fragments (Fig. 3I). The observed thickness of this layer is only 20-40cm in the outside section and about 400cm in the cave section (Fig. 2B). Its total thickness could not have been measured because in both cases the upper boundary is erosive. The observable structure of the lapilli tuff documents its origin in an ash and pumice flow (ignimbrite). Pedogenesis and weathering of the outside sections is accompanied with lateral changes in coloration from light gray to yellow and presence of ferric oxides. Samples were taken from the outside section, with a single exception of the lapilli tuff, which was sampled from an exfoliated part of the ignimbrite inside the cave.

Well preserved fossil leaves occur mainly at the boundary between fine-grained and coarse- grained tuff in the outside sections. Other plant remains were found close to the cave bottom and within the tuff.

The Lipovany section is situated in an abandoned sandpit (GPS: N 48.22606º, E 19.71610º) between the Mučín and Lipovany villages (Figs. 1-2; 4). The section starts with locally well cemented sandstones with glauconite at the base of the sandpit. They are followed by several meters of trough cross-bedded sandstones to conglomerates (facies St, Gt; Fig. 2B) belonging to the Bukovinka Fm. (Figs. 2B; 4E). Scour structures and mud rip-up clasts are present. These sandstones and conglomerates crop out at the bottom level of the sandpit (Fig. 4A). The second level of the sandpit is formed by light gray tuffs (Lt; Fig. 2B), which show poor sorting and circa 3-5mm pumice fragments and carbonized plant fragments (Fig. 4A-D). Grain size increases upward, but the tuffs are visibly finer than in the Mučín locality. Tuff is divided into several parallel layers, probably due to sheet jointing (Fig. 4C). Observable total thickness of tuffs is approximately 140cm, but their upper boundary is formed by recent soil. Unweathered tuff occurs in the central part of the second level. The samples for petrographical analysis and $^{40}Ar/^{39}Ar$ dating were taken from the fresh, Lt tuff (Figs. 2B; 4B, D). Thin section were made from a tuff affected by pedogenesis, and from the underlying, well cemented sandstones which are present at the base of the sandpit.

Petrographic description

Based on the sedimentological results, three different tuff lithotypes were described: fine grained tuff (Ft), sandy grained tuff (Ct), both only in Mučín locality and lapilli tuff (Lt; Mučín and Lipovany; Fig. 2). Petrographic composition of tuff from both localities is very similar.

The texture is crystallovitroclastic, composed of glass shards, pumice fragments and crystalloclasts of plagioclase, quartz and biotite (Fig. 5). Apatite, allanite, zircon and ilmenite are rare. Plagioclase crystalloclasts often contains adhering glass (Fig. 5B). Pumice fragments often have flattened vesicles and rarely contain phenocrysts of plagioclase or biotite (Fig. 5A). Accidental clasts are mainly made of mudstones; cognate recrystallized volcanic glass and vitrophyric volcanic lithoclasts are rare (Fig. 5G, H). Some muscovite is also present. Main differences between lithotypes and localities are grain-size and degree of alteration. Dated, fine tuff in the Mučín section is significantly altered to clay minerals (Figs. 2C-D; 3E; Appendix II). In the sandy tuff the amount of clay minerals is negligible due to good sorting. The content of quartz is higher, where a part of the grains is well rounded. Biotite crystalloclasts are often bended around dense grains. Lapilli tuffs shows larger admixture of accidental mudstone clasts. In the Mučín locality, all primary biotites are deficient at interlayer position due to the alteration into clay mineral (Table 2; Figs. 5E; 6). Dated Lipovany lapilli tuffs, contain fresh or slightly altered biotite crystalloclasts, which are annite in composition (Table 2; Figs. 5F; 6; Appendix II). Especially the small crystalloclasts of biotite lack visible alteration. But, the large biotite crystalloclasts show alteration along cleavability. In all lithotypes, plagioclase is dominated by andesine (Anorthite$_{25-55}$, Table 3; Fig. 7). Additionally, large crystalloclasts from the lapilli tuff show zonation with more basic central part (An_{78-72}, Figs. 5C-D; 7). One plagioclase crystalloclast from the Mučín lapilli tuff contains sieve texture with An_{42} core overgrown by An_{78} to An_{29} in rim (Fig. 5C), that documents input of a more basic magma in the magma chamber. Phenocrysts of sanidine were found only in rare cognate, vitrophyric volcanic lithoclasts (Figs. 5H; 7; Table 3). Mudstone lithoclasts contain quartz, albite, K-feldspar, muscovite, biotite/chlorite and sphene in clay matrix (Fig. 5G).

The amount of volatile components in the tuff is relatively high, especially in the markedly altered fine grained tuff from the Mučín section (16.5wt%; Table 4). Less altered fine tuff from the same layer consist of 13.0-10.7% volatiles. Ignimbrite tuffs contain only 6.6-8.1% of volatiles on both localities. The content of total carbon varies between 0.1-1% in all samples, which is influenced by the presence of carbonized plant fragments and leaves. However, the content of volatiles and total carbon questions their classification in the Total Alkali-Silica (TAS) diagram (Le Bas *et al.,* 1986) and other diagrams based on major elements (*e.g.* Peccerillo and Taylor, 1976). Therefore, the diagrams using trace elements are preferred for chemical classifications (Hastie *et al.,* 2007; Pearce, 1996). Based on whole rock chemical composition, studied samples belong to rhyodacitic volcanic rocks of high-K calc-alkaline series (Fig. 8). However, the tuff samples contain large amount of glass shards and pumice fragments. Thus, parental lava could have been more basic. The samples show medium Eu anomaly (0.53-0.68; Table 4; Fig. 8). The trace elements pattern (La_N/Yb_N, Zr/Y, Ba, Rb, Sr) indicate an origin within continental arc volcanism on a thick continental margin (*e.g.* Bailey, 1981).

Additionally, there are well observable trend that show loss of mobile, major elements in the TAS diagram (Fig. 8),

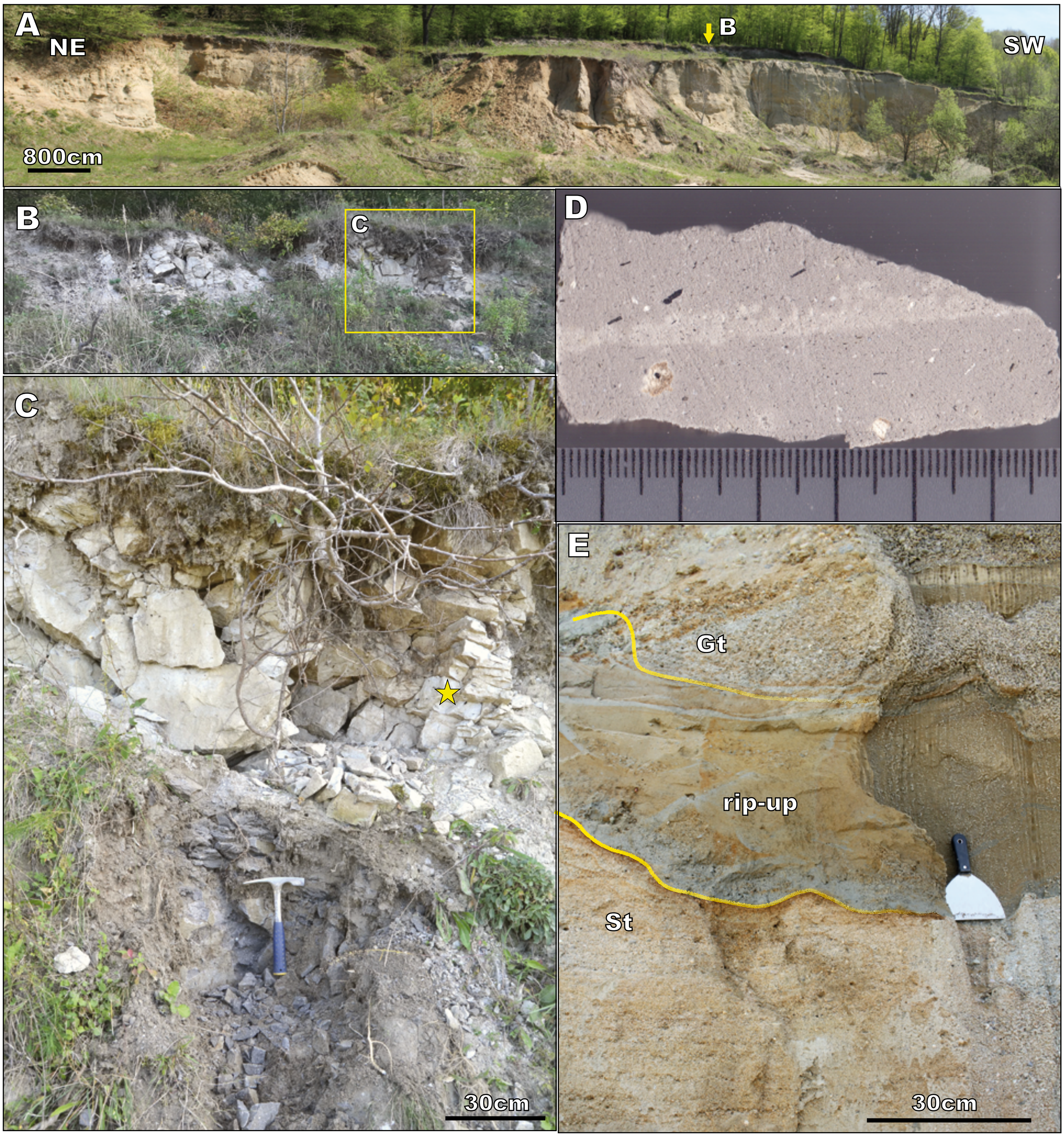

FIGURE 4. Lipovany section: A) general view, B) second level of sandpit with outcropped tuff, C) detailed section with the $^{40}Ar/^{39}Ar$ sample position marked by star, D) dated sample, E) detail of underlying deposits of the Bukovina Fm. (first level of sandpit; for abbreviation see Figure 2).

which reflect the alteration degree of the studied samples. In more altered, yellowish-ocher colored parts, the content of ferric oxide increases and the content of SiO_2, K_2O and Na_2O decreases. The slightly different trend is observed in chemical composition of vitroclasts, where alkali loss leads to higher relative content of SiO_2 (Table 5; Fig. 8). Although this trend is general, the position of samples in the TAS diagram is also affected by process of the probe analysis (see measurement condition in the Methods chapter). Data obtained with respect to elimination of mobile element loss during measurement provide more reliable result.

For better interpretation of non-volcanic admixture, the two samples from the underlying formation were

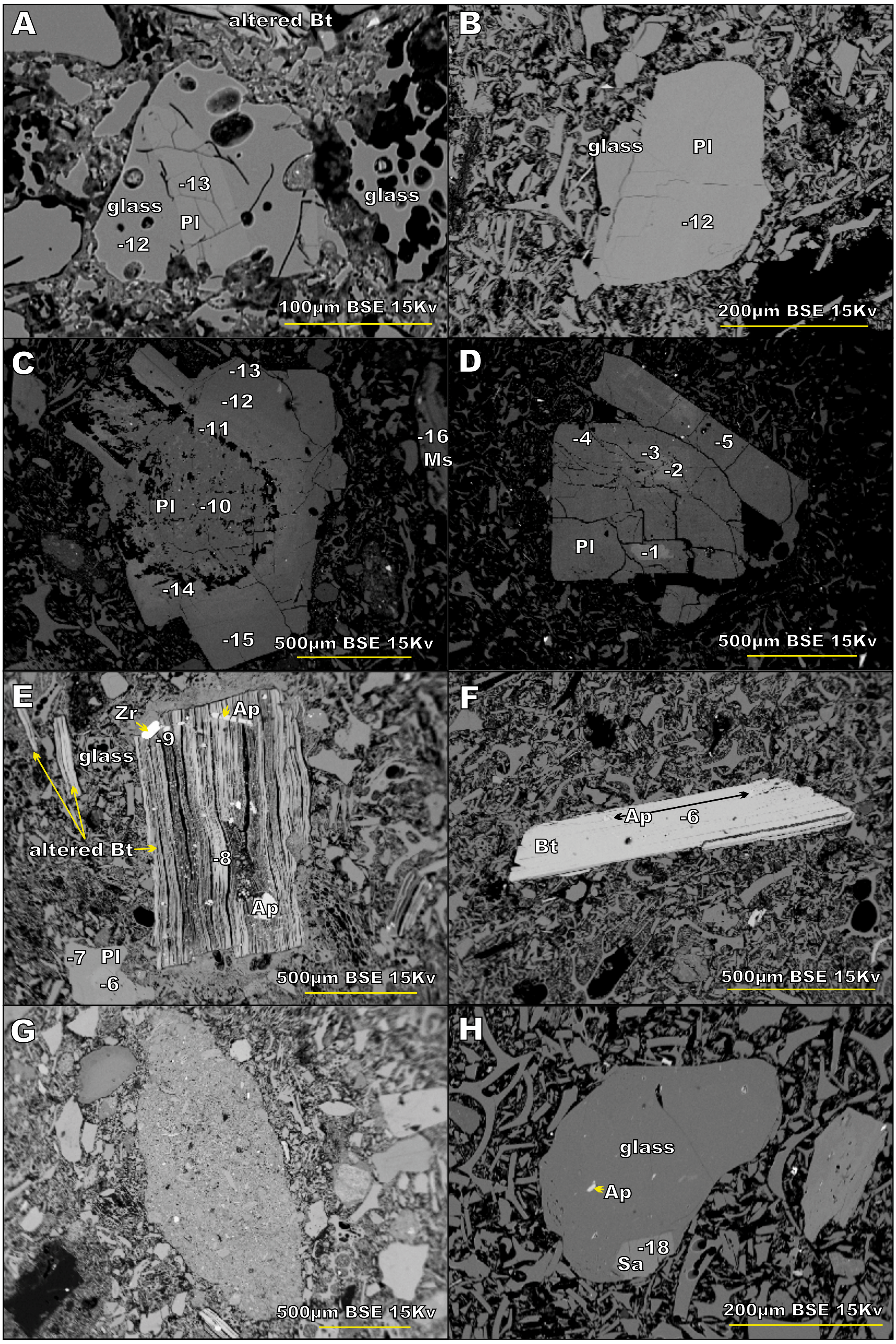

FIGURE 5. Back-scattered electrons (BSE) images of studied tuff: A) plagioclase (Pl) phenocryst within pumice fragment (Mučin-fine grained tuff), B) plagioclase crystalloclast with adhering glass (Lipovany), C) zonal plagioclase crystalloclast with sieve texture (Mučín-lapilli tuff), D) zonal plagioclase crystalloclast (Lipovany), E) altered biotite (Bt) crystalloclast with apatite (Ap) and zircon (Zr) inclusions (Mučín-lapilli tuff), F) biotite crystalloclast (Lipovany), G) mudstone lithoclasts (Mučín-lapilli tuff), H) volcanic lithoclasts with sanidine (Sa) phenocryst (Lipovany).

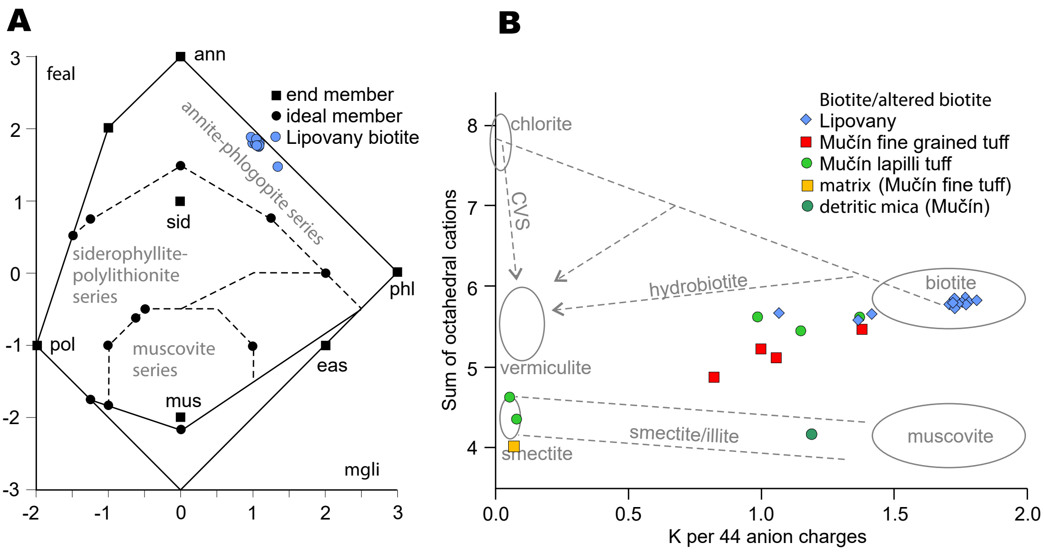

FIGURE 6. Composition of feldspars: A) Lipovany section; B) Mučín sections.

also analyzed. In the Mučín locality the underlying dark mudstones (silty claystones) are unsorted and composed of mono- polycrystalline quartz, feldspar, muscovite, biotite, felzite/silicite, and glauconite grains in a clay matrix. Mudstone contains 1.6% of Total Organic Carbon (TOC) and show kerogen type IV (HI 23.7mg HC/gTOC; Tmax 429ºC; S1 0.06mg HC/g rock, S2 0.38mg HC/g rock), which support terrestrial deposition with severe oxidation of organic matter. In the Lipovany section only the cemented sandstones from the base of the outcrop were analyzed. The sandstone is sorted and composed of subangular grains of quartz, K-feldspar, plagioclase, mica, felzite/silicite, schist, carbonate, glauconite and rare fossils cemented by calcite. Monocrystalline quartz dominate the mineral assemblage, but polycrystalline quartz is also present. K-feldspar show various degree of sericitization. Mica is represented by muscovite, chlorite and biotite.

$^{40}Ar/^{39}Ar$ results

A sample from the Lipovany ignimbrite was selected for radioisotopic dating due to its low degree of alteration. Based on the petrological observations, biotite and plagioclase were analyzed. In both cases, 15 measurements

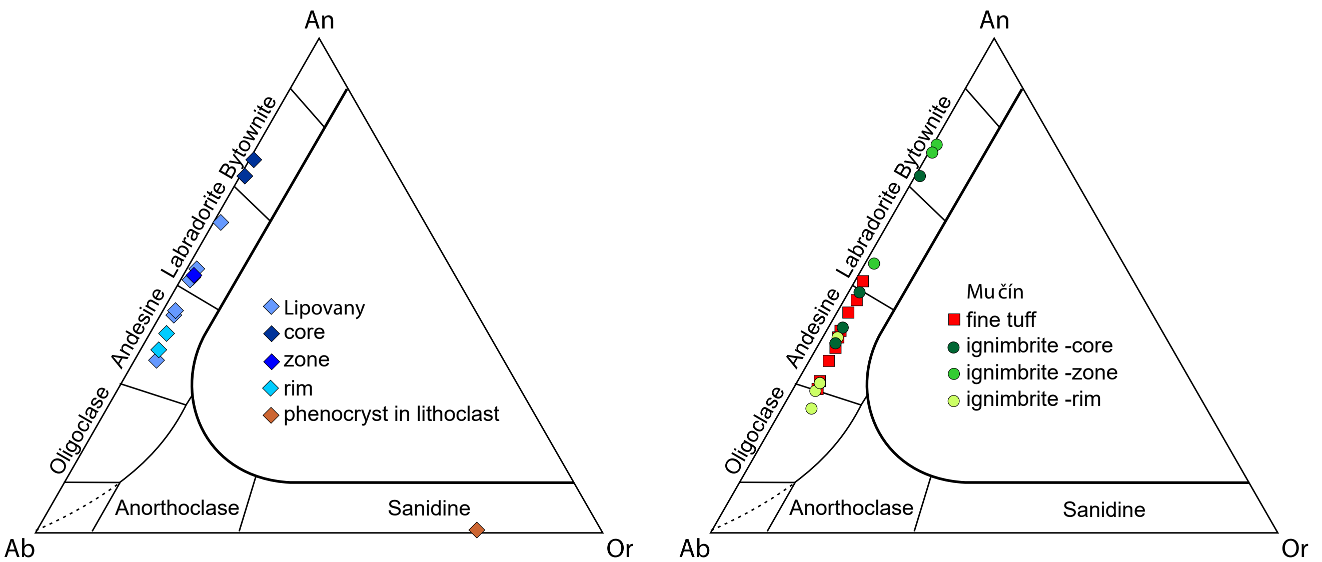

FIGURE 7. Mica analyses A) classification of Lipovany biotite (after Tischendorf *et al.*, 2007). B) Biotite alteration trends (after Jeong *et al.*, 2011). Abbreviation: CVS= interstratified chlorite-smectite/vermiculite.

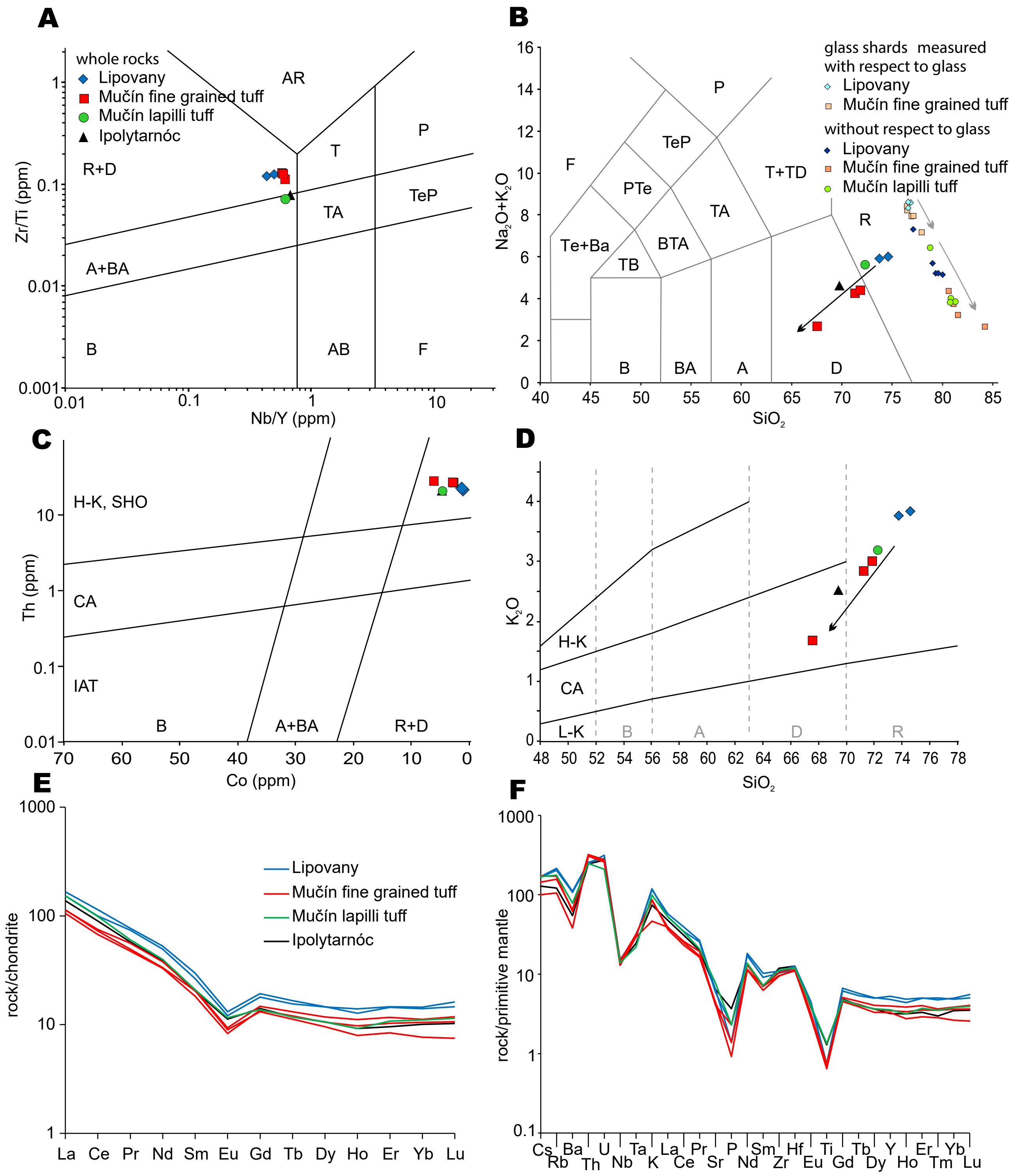

FIGURE 8. Chemical composition of the studied tuff. A) Classification diagram of volcanic rocks based on trace elements (Pearce, 1996), B) TAS diagram (Le Bas *et al.*, 1986), black arrows show weathering trend of whole rock samples. Gray arrows show weathering trend of volcanic glass. Note, glass shards were measured in two different condition (see methods). C) Classification diagram of volcanic series based on trace elements (Hastie *et al.*, 2007), D) Classification diagram of volcanic series based on major oxides (Peccerillo and Taylor, 1976), black arrows show weathering trend of whole rock samples. E) REE patterns of studied tuff (chondrite normalization value after Sun and McDonough, 1989), F) Trace element patterns (normalized after Sun and McDonough, 1989); Abbreviation: B= Basalt, A= Andesite, D= Dacite, R= Rhyolite, T=Ttrachyte, P= Phonolite, Te= Tephrite, F= Foidite, H-K= High K calc-alkaline series, CA= Calc Alkaline series, L-K= Low K calc alkaline series, SHO= Shoshonitic series, IAT= Island Arc Tholeiites.

TABLE 2. Representative analysis of biotites/altered biotites and matrix (Calculated based on 12 anions, normalized on the 22 cation charge). Abbreviations: I def.= interlayer-deficient mica (see Rieder *et al.*, 1998)

	Mučín-lapilli tuff			Mučín-fine tuff			Lipovany lapilli tuff							
	an8	an9	an19	an10	an11	an18	an1	an2	an5	an6	an7	an8	an9	an6_2
grain	bt2-z.1	bt2-z.2	bt3	bt3	bt4	matrix	bt1	bt2	bt4-z1	bt4-z.2	bt5	bt6-z.1	bt6-z.2	bt11
SiO_2	39.45	43.07	35.67	43.10	39.96	50.62	34.89	35.24	34.21	37.84	34.71	38.50	34.62	34.56
TiO_2	3.85	1.00	4.08	2.74	3.28	0.13	3.72	4.18	3.66	3.38	4.13	3.11	3.71	3.70
Al_2O_3	13.65	11.27	12.18	13.01	13.03	14.54	13.63	13.97	13.33	11.86	13.61	11.18	13.43	13.80
Cr_2O_3	0.01	0.01	0.03	0.02	0.00	0.00	0.01	0.01	0.00	0.01	0.08	0.02	0.00	0.02
FeO	19.24	11.60	21.02	17.05	20.27	5.10	23.37	24.29	23.39	20.33	23.62	21.99	23.37	23.58
MgO	7.33	1.72	7.38	6.16	7.84	2.26	9.15	8.52	9.11	8.16	8.73	7.34	9.01	9.19
MnO	0.16	0.00	0.15	0.18	0.25	0.03	0.24	0.16	0.25	0.18	0.18	0.10	0.23	0.22
NiO	0.00	0.00	0.02	0.00	0.00	0.02	0.02	0.00	0.00	0.00	0.00	0.00	0.00	0.00
CaO	0.36	0.83	0.29	0.59	0.23	1.30	0.01	0.07	0.03	0.26	0.00	0.14	0.09	0.05
K_2O	5.72	0.23	6.44	5.30	6.94	0.33	8.79	8.53	8.82	6.58	8.74	5.09	8.46	8.51
Na_2O	0.02	0.03	0.04	0.17	0.15	0.22	0.38	0.43	0.40	0.04	0.45	0.04	0.37	0.40
Cl	0.23	0.19	0.20	0.17	0.23	0.17	0.22	0.22	0.20	0.16	0.20	0.15	0.20	0.19
F	0.00	0.00	0.00	0.00	0.00	0.00	0.00	0.00	0.00	0.00	0.00	0.00	0.00	0.00
Total	90.03	69.94	87.50	88.48	92.18	74.75	94.44	95.64	93.39	88.82	94.46	87.67	93.49	94.22
Total-cl. f	89.97	69.89	87.45	88.44	92.13	74.71	94.39	95.59	93.35	88.79	94.41	87.64	93.45	94.17
Si	3.099	3.919	2.967	3.360	3.105	4.075	2.763	2.758	2.749	3.070	2.752	3.153	2.768	2.743
Al	0.901	0.081	1.033	0.640	0.895	0.000	1.237	1.242	1.251	0.930	1.248	0.847	1.232	1.257
Sum T	*4.000*	*4.000*	*4.000*	*4.000*	*4.000*	*4.075*	*4.000*	*4.000*	*4.000*	*4.000*	*4.000*	*4.000*	*4.000*	*4.000*
Al	0.362	1.127	0.162	0.555	0.298	1.380	0.035	0.046	0.011	0.204	0.024	0.232	0.033	0.034
Ti	0.227	0.068	0.255	0.161	0.192	0.008	0.222	0.246	0.221	0.207	0.247	0.192	0.223	0.221
Fe	1.264	0.882	1.462	1.111	1.318	0.343	1.548	1.590	1.572	1.379	1.566	1.506	1.563	1.565
Mg	0.858	0.233	0.915	0.716	0.908	0.271	1.081	0.994	1.091	0.987	1.032	0.896	1.074	1.088
Mn	0.010	0.000	0.011	0.012	0.016	0.002	0.016	0.011	0.017	0.013	0.012	0.007	0.016	0.015
Cr	0.001	0.001	0.002	0.001	0.000	0.000	0.001	0.001	0.000	0.001	0.005	0.001	0.000	0.001
Ni	0.000	0.000	0.001	0.000	0.000	0.001	0.001	0.000	0.000	0.000	0.000	0.000	0.000	0.000
sum M	*2.723*	*2.312*	*2.808*	*2.556*	*2.732*	*2.006*	*2.904*	*2.887*	*2.913*	*2.790*	*2.886*	*2.834*	*2.909*	*2.924*
Ca	0.031	0.081	0.026	0.049	0.019	0.112	0.001	0.006	0.003	0.023	0.000	0.012	0.008	0.005
K	0.573	0.026	0.684	0.527	0.688	0.034	0.889	0.852	0.904	0.681	0.884	0.532	0.863	0.862
Na	0.003	0.005	0.006	0.025	0.022	0.035	0.058	0.065	0.062	0.007	0.070	0.007	0.057	0.061
sum I	*0.607*	*0.112*	*0.716*	*0.601*	*0.729*	*0.181*	*0.947*	*0.923*	*0.969*	*0.710*	*0.953*	*0.551*	*0.927*	*0.927*
	I def.	clay	I def.	I def.	I def.	clay	annite	annite	annite	I def.	annite	I def./clay	annite	annite

TABLE 3. Representative analysis of plagioclase (Calculated based on 8 oxygen)

	Mučín lapilli tuff						Mučín fine tuff				Lipovany lapilli tuff				
analyse	an10	an11	an12	an13	an14	an15	an1	an3	an13	an12	an2	an3	an4	an5	an18
grain	3core	3z.1A	3z.2A	3rimA	3z.1B	3rimB	1	3	8	3	1core	1zone	1rim	2	lithoc.
SiO_2	57.22	48.01	53.42	60.09	48.01	60.82	56.35	60.86	56.72	56.86	48.86	54.70	58.79	58.22	65.10
Al_2O_3	26.93	32.65	28.75	24.82	32.91	24.76	26.87	23.78	27.01	26.47	31.84	27.81	25.27	25.96	18.42
SrO	0.07	0.07	0.11	0.07	0.07	0.04	0.07	0.06	0.06	0.08	0.12	0.07	0.07	0.06	0.04
FeO	0.18	0.25	0.16	0.15	0.30	0.15	0.32	0.19	0.20	0.20	0.18	0.20	0.17	0.22	0.11
MgO	0.01	0.02	0.01	0.00	0.00	0.00	0.01	0.01	0.00	0.00	0.00	0.01	0.00	0.00	0.01
CaO	8.65	15.71	11.23	6.38	15.69	6.08	9.71	6.43	9.26	9.18	15.40	10.62	7.73	8.25	0.15
Na_2O	6.42	2.53	5.00	7.60	2.31	7.84	5.83	7.64	6.10	5.96	2.69	5.17	6.87	6.40	2.41
K_2O	0.43	0.09	0.25	0.70	0.09	0.71	0.40	0.70	0.37	0.36	0.11	0.30	0.55	0.49	12.93
Total	99.91	99.32	98.93	99.81	99.39	100.40	99.56	99.68	99.71	99.11	99.20	98.88	99.45	99.60	99.17
Si	2.572	2.216	2.443	2.687	2.212	2.701	2.549	2.724	2.557	2.576	2.254	2.495	2.646	2.618	2.999
Al	1.426	1.776	1.550	1.308	1.787	1.296	1.433	1.255	1.435	1.413	1.731	1.495	1.340	1.376	1.000
Sr	0.002	0.002	0.003	0.002	0.002	0.001	0.002	0.002	0.002	0.002	0.003	0.002	0.002	0.001	0.001
Fe	0.007	0.009	0.006	0.006	0.011	0.006	0.012	0.007	0.007	0.008	0.007	0.008	0.006	0.008	0.004
Mg	0.000	0.001	0.000	0.000	0.000	0.000	0.000	0.001	0.000	0.000	0.000	0.001	0.000	0.000	0.000
Ca	0.416	0.777	0.550	0.306	0.775	0.289	0.471	0.309	0.447	0.446	0.761	0.519	0.373	0.398	0.008
Na	0.560	0.226	0.443	0.659	0.207	0.675	0.512	0.663	0.533	0.524	0.240	0.457	0.600	0.558	0.215
K	0.025	0.005	0.015	0.040	0.006	0.040	0.023	0.040	0.021	0.021	0.006	0.017	0.032	0.028	0.760
Cat sum	*5.007*	*5.012*	*5.011*	*5.008*	*5.000*	*5.009*	*5.002*	*5.000*	*5.003*	*4.989*	*5.004*	*4.994*	*4.999*	*4.987*	*4.988*
Or	2.46	0.54	1.47	3.96	0.56	4.01	2.28	3.95	2.12	2.08	0.62	1.74	3.16	2.86	77.36
Ab	55.92	22.44	43.96	65.63	20.94	67.22	50.91	65.54	53.21	52.90	23.85	46.03	59.72	56.72	21.86
An	41.61	77.02	54.57	30.41	78.50	28.77	46.81	30.50	44.67	45.03	75.53	52.23	37.12	40.43	0.77

were made (Appendix I.I-II). Generally, due to the low potassium content (ca. 0.05-0.1wt%; Verati and Jourdan, 2014), plagioclase is less suitable for single crystal total fusion $^{40}Ar/^{39}Ar$ dating but the analysis single crystal is necessary due to the possibility of crystal inheritance in tuff rocks. In this case no sanidine crystals were present, and as indicated by low K/Ca values, only plagioclase could be analyzed. For the age calculation, only the nine youngest plagioclase grains were used whereas the oldest crystals were interpreted as inherited from previous eruptions. The obtained converging age of 17.49±0.54Ma (n= 9; P= 0.96) is supported by an inverse isochron age of 17.3±1.1Ma with a trapped ratio of 305±28, indistinguishable from atmospheric value, and a P-value of 0.95 (Fig. 9A-B, Appendix I.I). Omitted analyses with older ages have similar K/Ca and $^{40}Ar(r)$ values and fail to align on a common inverse ischron mixing line (Fig. 9B). It suggests their source in older deposits incorporated into pyroclastic flow. On the other hand, only six oldest biotites were used for the age calculation (Appendix I.II). Other biotite crystal have likely been affected by alteration, which is indicated by the their low radiogenic $^{40}Ar^{*}$ values and therefore, high content in atmospheric Ar. The biotite converge toward an age of 17.28±0.06Ma with probability of fit 0.11. Inverse isochron give an age of 17.29±0.10Ma with probability 0.07 (Fig. 9C-D; Appendix I.II).

Second sample was taken from lower fine grained tuff of the Mučín section. As is mentioned above, the Mučín locality yields high degree of alteration. From this point of view, biotites are not suitable for measurements. However, this fine tuff contains the majority of the fossil leaves in its upper boundary and therefore it was selected for $^{40}Ar/^{39}Ar$ dating. From 15 plagioclase analyses, only nine with $^{40}Ar(r)> 35\%$ were used for age calculation (Appendix I.III) as the other younger crystals have likely been altered. The calculated a convergent age of 16.5±1.4Ma with a probability of fit of 0.32 (Fig. 9E-F; Appendix I.III) shows the relatively large uncertainty being due to the small crystal sizes and therefore the small (close-to-background level) ^{40}Ar signal generated by each crystal.

DISCUSSION

All studied tuffs are crystallovitroclastic and rhyodacitic in composition. They have similar mineralogical and geochemical properties. Small differences can be explained by different grain size and degree of alteration. From this point of view, tuffs from both localities represent probably a single event. The three different lithotypes observed at the Mučín section (Ft, Ct, Lt; Fig. 2C, D) can be interpreted as follows. The basal fine grained tuff (Ft) with indistinct gradation represents an ash fall deposit. The origin of the sandy grained tuff (Ct) is more difficult to interpret because of its poor exposure. The presence of high amount of quartz grains, good sorting and the occurrence of few sandstone pebbles (Fig. 3E) indicate transport and deposition by a flash flood (reworking) or by a pyroclastic surge. In both cases, part of the quartz grains and the rare pebbles were sourced from the underlying sediments. If the reworking by a flash flood is true, the correct petrographic term for this lithotype is volcanic sandstone. However, deposits of pyroclastic surges are common at the base of dense pyroclastic flows. Such pumice pyroclastic flow is interpreted in the overlying lapilli tuff layer (Lt) with inverse gradation. Regardless of the sandy layer origin, these sediments were deposited immediately after each other. The lapilli tuff (Lt) from Lipovany also shows structural signs of a pyroclastic flow (absence of sorting, inverse grading, and carbonized plant fragments). Considering the similar mineralogical and geochemical composition of these deposits, it probably represents lateral continuation of the Mučín ignimbrite layer. However, the boundary between the ignimbrite

TABLE 4. Whole rock analysis of tuffs (n.d.= sample under detection limit)

sample	Lipovany		Mučín fine tuff			M.lapilli	Ipoly
SiO_2	69.54	67.67	63.52	56.36	62.45	67.20	62.1
TiO_2	0.16	0.16	0.15	0.16	0.14	0.29	0.28
Al_2O_3	13.50	13.58	14.66	14.54	14.17	14.41	15.00
Fe_2O_3	1.91	2.39	4.01	6.53	3.50	2.89	3.64
Cr_2O_3	n.d.	n.d.	n.d.	n.d.	n.d.	n.d.	0.005
MgO	0.73	0.76	1.34	1.79	1.27	0.70	1.54
MnO	0.04	0.04	0.03	0.02	0.03	0.04	0.04
CaO	1.67	1.69	1.54	1.73	1.49	2.13	2.43
Na_2O	2.02	1.96	1.27	0.83	1.21	2.28	1.89
K_2O	3.58	3.46	2.54	1.40	2.61	2.98	2.23
P_2O_5	0.05	0.03	0.05	0.03	0.02	0.05	0.08
Sum	93.2	91.74	89.11	83.39	86.89	92.97	89.235
LOI	6.6	8.1	10.7	16.5	13.0	6.9	10.6
Rb	128.9	136.0	108.3	66.8	99.6	111.5	77.0
Sr	124.5	135.6	85.9	93.8	88.8	163.2	135.7
Ba	747	769	431	266	452	547	380
Co	1.2	1.3	6.1	2.7	2.8	4.7	4.9
Nb	10.5	10.9	10.5	9.2	9.4	9.9	9.9
Ta	1.2	1.2	1.3	1.2	1.3	0.9	1.0
Ga	13	13.6	13.3	13.2	12.6	14.3	13.2
Hf	3.5	3.9	3.7	3.4	3.5	3.7	3.9
Th	21.0	21.7	27.2	26.0	26.9	21.0	20.7
U	6.6	6.0	5.8	5.4	5.6	4.4	5.7
V	16	21	13	15	16	34	43
Zr	115.2	121.5	116.7	107.2	105.9	126.2	132.8
La	36.2	39.4	26.7	26.9	25.0	36.1	32.7
Ce	61.1	69.8	45.9	44.3	41.2	60.5	55.0
Pr	7.01	7.33	5.33	4.69	4.50	5.73	5.48
Nd	23.1	24.6	17.7	15.6	15.4	18.6	17.9
Sm	4.04	4.53	3.18	3.13	2.78	3.20	3.11
Eu	0.70	0.76	0.54	0.52	0.48	0.67	0.65
Gd	3.67	3.96	3.02	2.69	2.78	2.82	2.89
Tb	0.58	0.62	0.49	0.42	0.45	0.44	0.44
Dy	3.68	3.71	2.98	2.43	2.67	2.70	2.68
Ho	0.79	0.72	0.63	0.45	0.55	0.52	0.52
Er	2.41	2.38	1.93	1.39	1.70	1.78	1.58
Tm	0.35	0.37	0.27	0.21	0.26	0.26	0.22
Yb	2.46	2.38	1.90	1.30	1.78	1.87	1.71
Y	24.0	21.9	18.1	14.9	15.8	16.2	14.5
Lu	0.41	0.37	0.30	0.19	0.27	0.29	0.26
C_{tot}	0.71	0.23	1.01	0.43	0.25	0.14	0.29
S_{tot}	n.d.	n.d.	n.d.	n.d.	n.d.	n.d.	0.3
Eu*	0.56	0.55	0.53	0.55	0.53	0.68	0.66
La_N/Yb_N	10.56	11.87	10.08	14.84	10.07	13.85	13.72

and the underlying terrestrial sediments does not crop out now in the Lipovany section. Previous paleontological works did not contain a lithological column and detailed description of the fossiliferous Lipovany tuff is absent (Němejc and Knobloch, 1969, 1973; Sitár and Kvaček, 1997). Other regional works described some vertical and lateral changes (Kuthan ed., 1963; Vass and Elečko, 1992).

Two $^{40}Ar/^{39}Ar$ ages of 17.49±0.54Ma (plagioclase) and 17.28±0.06Ma (biotite) obtained from the Lipovany tuff are indistinguishable within uncertainties (Fig. 9A-D; Appendix I.I-II) and therefore, the most probable eruption age is best represented by the more precise biotite age of 17.28±0.06Ma. The $^{40}Ar/^{39}Ar$ convergent age of 16.5±1.4Ma from the fine grained Mučín tuff, which underlies the

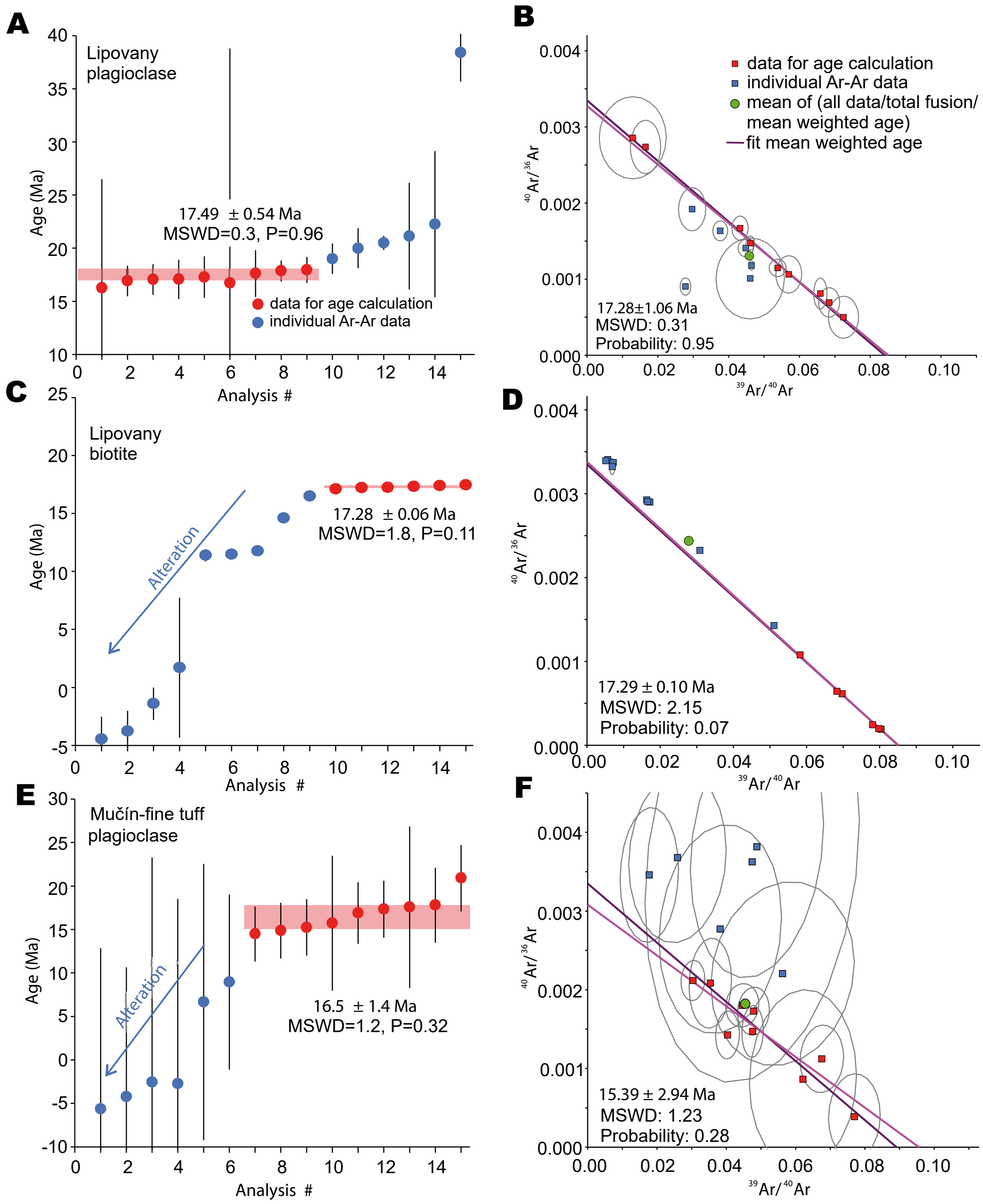

FIGURE 9. Result of $^{40}Ar/^{39}Ar$ dating: A-B) Plagioclase converging age and inverse isochron diagrams (Lipovany section), C-D) Biotite converging age and inverse isochron diagrams (Lipovany section), E-F) Plagioclase converging age and inverse isochron diagrams from the (Mučín fine grained tuff).

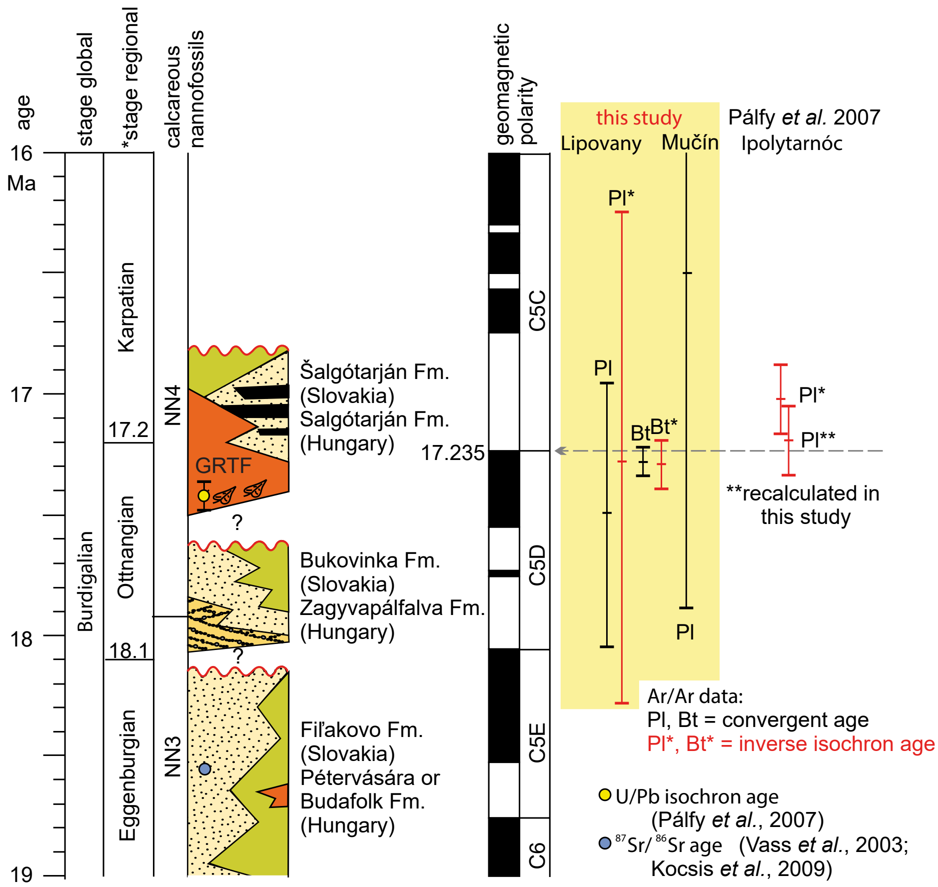

FIGURE 10. Correlation of age results. Note, that the gained ages is the same as the normal and reverse chron boundary described by Márton et al. (2007); For abbreviations see Figure 2.

ignimbrite, shows a large error due to the low K-content and small crystal size of plagioclase (and consequently low ^{40}Ar yield during measurement). Although the ages of both tuffs overlap, due to the large uncertainty of the Mučín tuff age, it cannot be unequivocally defined if all tuffs are of the same age or if they come from several consecutive volcanic events. Although the data cannot be clearly linked, they strictly indicate deposition of these tuffs close to the Ottnangian/Karpatian boundary according to Harzhauser et al. (2019). Additionally, our new ^{40}Ar/^{39}Ar data fit well with a single-crystal laser-fusion plagioclase ^{40}Ar/^{39}Ar age of 17.02±0.14Ma (Pálfy et al., 2007; Fig. 10). Especially if the ^{40}Ar/^{39}Ar age of Pálfy et al. (2007) is recalculated to 17.19±0.14Ma using the constants of Renne et al. (2011) adopted in this study, and which are fully calibrated against the U-Pb system (Renne et al., 2010). Our age is further supported by the single-crystal zircon U–Pb isochron age of 17.42±0.04Ma from Ipolytarnóc (Pálfy et al., 2007). Because of extremely high closure temperature of zircon, this U-Pb age probably document zircon crystallization in magma chamber and therefore it is possible that this age include data point from antecrysts zircon crystals (Schaltegger and Davies, 2017).

Based on these results, the previous stratigraphic interpretations of the Lipovany tuff based on magnetostratigraphy may be rejected (Márton et al., 2007; Vass et al., 2006). These authors ranked the Mučín section with normal polarity chron C5Dn (Hilgen et al., 2012) to the Ottnangian and Lipovany section (marked as NE Lipovany in Vass et al., 2006 and Márton et al., 2007) with reversed polarity (C5Er) to the Eggenburgian. However, the new ^{40}Ar/^{39}Ar data from NE Lipovany section, produced by this study, date the studied deposits as late Ottnangian in age. Moreover similar result was also presented by Pálfy et al. (2007) from the Ipolytarnóc (normal polarity) and Nemti tuff (reversal polarity; Márton et al., 2007; Vass et al., 2006). Pálfy et al. (2007) concluded that both mentioned localities are indistinguishable in age and petrography. Furthermore, such units usually have wide distribution, therefore these authors concluded that both tuffs represent a single ignimbrite eruption. It must be mentioned here, that only first two ignimbrite sheets from the Ipolytarnóc show normal polarity and the third displays reverse polarity (Márton et al., 2007). It can be noted, that the assumed age of 17.28±0.06Ma (this study) fit with C5D-C5C magnetochron boundary (Fig. 10).

TABLE 5. Representative probe analysis of glass shards and pumice fragments

condition						Silicate						glass	
	Mučín lapilli			Mučín fine tuff			Lipovany		Mučín fine tuff			Lipovany	
analyse	An4	An17	An18	An14	An15	An16	An20	An22	An2	An3	An4	An5	An6
SiO_2	76.55	76.10	76.12	74.61	73.45	77.10	75.65	74.87	71.96	71.94	70.32	72.28	71.82
TiO_2	0.02	0.03	0.03	0.03	0.03	0.02	0.05	0.04	0.02	0.04	0.06	0.07	0.04
Al_2O_3	12.27	12.44	12.36	11.91	11.75	12.41	12.18	12.09	11.80	12.05	12.01	12.03	11.97
Cr_2O_3	0.00	0.00	0.00	0.00	0.02	0.00	0.00	0.00	0.00	0.00	0.00	0.01	0.00
MgO	0.04	0.05	0.06	0.05	0.05	0.05	0.06	0.10	0.05	0.06	0.05	0.00	0.04
FeO	0.77	0.84	0.76	0.89	0.82	0.84	0.77	0.90	0.82	0.88	0.82	0.70	0.81
MnO	0.06	0.04	0.05	0.06	0.07	0.04	0.06	0.11	0.05	0.11	0.07	0.02	0.08
NiO	0.00	0.01	0.01	0.00	0.00	0.00	0.00	0.00	0.00	0.02	0.00	0.00	0.00
CaO	0.73	0.96	0.81	0.82	0.83	0.86	0.80	1.01	0.84	0.80	0.89	0.84	0.86
K_2O	2.15	2.11	2.19	2.24	1.81	2.66	3.02	3.00	4.50	4.85	4.78	4.98	4.92
Na_2O	1.51	1.52	1.63	1.23	1.08	1.50	1.87	1.90	2.11	2.54	2.76	3.10	3.17
P_2O_5									0.00	0.00	0.02	0.00	0.00
SO_3									0.00	0.01	0.00	0.01	0.00
Cl	0.12	0.13	0.13	0.12	0.13	0.12	0.10	0.10	0.13	0.15	0.12	0.07	0.10
Total	94.23	94.22	94.16	91.96	90.05	95.60	94.56	94.12	92.28	93.48	91.90	94.10	93.81
-O=Cl	0.03	0.03	0.03	0.03	0.03	0.03	0.02	0.02	0.03	0.03	0.03	0.02	0.02
Total(F.Cl)	94.20	94.19	94.13	91.93	90.02	95.57	94.54	94.10	92.25	93.44	91.88	94.08	93.79

Implication for paleoclimatology and stratigraphy context

As mentioned above, the majority of fossil leaves in Mučín section are present within the fine tuff (Ft) close to the boundary with the sandy tuff layer (Ct). Localization of fossil leaves at Lipovany is vaguely described as a bedded tuff or tuffite located in the upper part of sandpit (Němejc and Knobloch, 1969, 1973; Sitár and Kvaček, 1997). Despite imprecise $^{40}Ar/^{39}Ar$ data from Mučín fine grained tuff, the result from this study confirm late Ottnangian age of both fossil leaves associations. Then, the floral assemblages from both studied localities document Ottnangian climatic patterns as were presented by original authors (*e.g.* Kuthan, 1963; Němejc and Knobloch, 1969, 1973). These localities together with Ipolytarnóc can again be used as parastratotype of the Ottnangian regional stage as already suggested by Němejc and Knobloch (1973) and Hably (1985). Hence, previous works in which the Lipovany and Mučín fossil assemblages are interpreted as a late Eggenburgian must be reconsidered (*e.g.* Erdei *et al.*, 2007; Kučerová, 2009; Sitár and Kvaček, 1997; Vass and Elečko, 1992). Similarly, the interpretation of Márton *et al.* (2007), that rainforest vegetation from the studied localities is most probably younger than the swamp vegetation of the Salgótarján Formation is most likely not correct. The numerous papers described sediments and coal seams of Salgótarján Fm. in the overburden of the studied tuff (*e.g.* Bartkó, 1985; Kuthan, 1963; Pálfy *et al.*, 2007; Vass and Elečko, 1992). The most probable paleoenvironmental scenario is that the terrestrial sediments of the Bukovinka/Zagyvapálfalva Fm. formed a paleosurface overgrown by a humid subtropical forest as indicated by leaf assemblage (Hably, 1985; Kučerová, 2009; Němejc and Knobloch, 1973; Sitár and Kvaček, 1997). The catastrophic volcanic activity destroyed this ecosystem. The ash-fall deposits together with the ignimbrites buried the existing flora and fossil tracks and protected them against decay. Silica-rich hydrothermal fluids associated with the volcanic activity petrified tree trunks, which are common within the studied tuff and within the underlying Bukovinka/Zagyvapálfalva Fm. (*e.g.* Bartkó, 1985; Sitár and Kvaček, 1997; Vass and Elečko, 1992). Deposition of the Salgótarján Fm. followed, and was possibly affected by volcanism which triggered change in the local climate, morphology and edaphic conditions. In any case, climatic conditions remained subtropical, but floral assemblages changed to swamp forests in the Salgótarján Fm. (*e.g.* Nagy, 2005; Němejc, 1963; Planderová in Vass and Elečko, 1992). These climatic conditions represent the beginning of Miocene Climatic Optimum (Böhme, 2003; Sitár and Kvaček, 1997).

It should be noted that deposition of Salgótarján Fm. took place during latest Ottnangian and earliest Karpatian (Pálfy *et al.*, 2007; this study). Presence of *Sphenolitus belemnos* (Holcová, 2001) within Salgótarján Fm. must be interpreted as reworked from older strata. The Karpatian marine transgression in this area began around 17.3Ma, similarly as in the Vienna Basin (Harzhauser *et al.*, 2019). Dating of this event in Vienna Basin was set to 17.23±0.18Ma (Roetzel *et al.*, 2014), what was recalibrated using the constant of Renne *et al.* (2011) to 17.29± 0.18Ma (Table 1).

CONCLUSION

The new plagioclase and biotite $^{40}Ar/^{39}Ar$ ages of 17.49±0.54Ma and 17.28±0.06Ma, respectively, from the fossiliferous Lipovany tuff indicate that the volcanic eruption event took place during the latest Ottnangian up to the Ottnangian/Karpatian regional stage boundary (intra Burdigalian). Moreover, $^{40}Ar/^{39}Ar$ data together with magnetostratigraphy (end of C5Dn chron) supports this regional stage boundary.

The data supplements correlation of the fossil flora assemblage from the Ipolytarnóc, Mučín and Lipovany sites. In this area, the terrestrial environment was overgrown by subtropical rain forest which existed before the volcanic eruption. This environment was buried during a volcanic event associated with the formation of pyroclastic flows. The presented catastrophic event conserved these important fossil sites. After the eruption a subtropical swamp forest developed and lead to the deposition of Salgótarján Fm. Obtained data indicate that the deposition of Salgótarján Fm. is younger, with an age of about 17.3Ma.

ACKNOWLEDGMENTS

This research was supported by the Slovak Research and Development Agency under contracts No. APVV-16-0121, APVV-15-0575 and by the Scientific Grant Agency of the Ministry of Education, Science, Research and Sport of the Slovak Republic under the contract No. VEGA/1/0526/21 and VEGA/1/0346/20. The authors wish to express their gratitude to Prof. Huraiová for her donation of reference sample from Ipolytarnóc. We express gratitude to our editor and reviewers for insightful comments and suggestions.

REFERENCES

Bailey, J.C., 1981. Geochemical criteria for a refined tectonic discrimination of orogenic andesites. Chemical Geology, 32, 139-154.

Bartkó, L., 1985. Geology of Ipolytarnoc. Geologica Hungarica series, Palaeontologica, 44, 16-71.

Böhme, M., 2003. The Miocene Climatic Optimum: evidence from ectothermic vertebrates of Central Europe. Palaeogeography, Palaeoclimatology, Palaeoecology, 195, 389-401. DOI: https://doi.org/10.1016/S0031-0182(03)00367-5

Erdei, B., Hably, L., Kázmér, M., Utescher, T., Bruch, A.A., 2007. Neogene flora and vegetation development of the Pannonian domain in relation to palaeoclimate and palaeogeography. Palaeogeography, Palaeoclimatology, Palaeoecology, 253, 115-140. DOI: https://doi.org/10.1016/j.palaeo.2007.03.036

Fusán, O., Biely, A., Ibrmajer, J., Plančár, J., Rozložník L., 1987. Basement of the Tertiary of the inner West Carpathians. Bratislava, Geological Institute of Dionýz Štúr, 123pp.

Gyalog, L., Síkhegyi, F. (eds.), 2005. Geological map of Hungary, M= 1: 100,000. Budapest, Hungarian State Geological Institute. Website: https://map.mbfsz.gov.hu/fdt100/. Last accessed: August 2020.

Hably, L., 1985. Early Miocene plant fossils from Ipolytarnoc, N. Hungary. Geologica Hungarica series, Palaeontologica, 45, 78-255.

Hámor, G., Ravasz-Baranyai, L., Balogh, K., Árva-Sós, E., 1979. K/Ar dating of pyroclastic rocks in Hungary. Annales Géologiques des Pays Helléniques Tome hors série, 2, 491-500.

Harzhauser, M., Theobalt, D., Strauss, P., Mandic, O., Piller, W.E., 2019. Seismic-based lower and middle Miocene stratigraphy in the northwestern Vienna Basin (Austria). Newsletters on Stratigraphy, 52(2), 221-247. DOI: https://doi.org/10.1127/nos/2018/0490

Hastie, A.R., Kerr, A.C., Pearce, J.A., Mitchell, S.F., 2007. Classification of Altered Volcanic Island Arc Rocks using Immobile Trace Elements: Development of the Th-Co Discrimination Diagram. Journal of Petrology, 48(12), 2341-2357. DOI: https://doi.org/10.1093/petrology/egm062

Hilgen, F.J., Lourens, L.J., Van Dam, J.A., 2012. The Neogene Period. In: Gradstein, F.M., Ogg, J.G., Schmitz, M.D., Ogg, G.M. (eds). The Geologic Time Scale 2012. Amsterdam, Elsevier, Volume 2, 923-978. DOI: https://doi.org/10.1016/B978-0-444-59425-9.00029-9

Hók, J., Šujan, M., Šipka, F., 2014. Tectonic division of the Western Carpathians: An overview and a new approach. Acta Geologica Slovaca, 6, 135-143.

Holcová, K., 2001. New methods in foraminiferal and calcareous nannoplankton analysis and evolution of Oligocene and Miocene basins of the Southern Slovakia. Slovak Geological Magazine, 7(1), 19-41.

Horváth, F., Musitz, B., Balázs, A., Végh, A., Uhrin, A., Nádor, A., Koroknai, B., Pap, N., Tóth, T., Wórum, G., 2015. Evolution of the Pannonian Basin and its geothermal resources. Geothermics, 53, 328-352. DOI: https://doi.org/10.1016/j.geothermics.2014.07.009

Jeong, G.Y., Hillier, S., Kemp, R.A., 2011. Changes in mineralogy of loess–paleosol sections across the Chinese Loess Plateau. Quaternary Research, 75, 245-255. DOI: https://doi.org/10.1016/j.yqres.2010.09.001

Jourdan, F., Renne, P., 2007. Age calibration of the Fish Canyon sanidine $^{40}Ar/^{39}Ar$ dating standard using primary K–Ar standards. Geochimica et Cosmochimica Acta, 71, 387-402. DOI: https://doi.org/10.1016/j.gca.2006.09.002

Kocsis, L., Vennemann, T.W., Hegner, E., Fontignie, D., Tütken, T., 2009. Constraints on Miocene oceanography and climate in the Western and Central Paratethys: O-, Sr-, and Nd-isotope compositions of marine fish and mammal remains. Palaeogeography, Palaeoclimatology, Palaeoecology, 271, 117-129. DOI: https://doi.org/10.1016/j.palaeo.2008.10.003

Koppers, A.A.P., 2002. ArArCALC-software for $^{40}Ar/^{39}Ar$ age calculations. Computers & Geosciences, 28, 605-619. DOI: https://doi.org/10.1016/S0098-3004(01)00095-4

Kordos, L., 1985. Footprints in the Lower Miocene sandstone of Ipolytarnoc. Geologica Hungarica series, Palaeontologica, 46, 260-415.

Kučerová, J., 2009. Miocénna flóra z lokalít Kalonda a Mučín. Acta Geologica Slovaca, 1(1), 65-70.

Kuthan, M., Biely, A., Böhm, V., Čechovič, V., Fusán, O., Hovorka, D., Mazúr, E., Regásek, F., 1963. Vysvetlivky kprehľadnej geologickej mape ČSSR 1:200 000, M-34-XXXII Zvolen. Geofond Bratislava, 132pp.

Le Bas, M.J., Le Maitre, R.W., Strecheisen, A., Zanettin, B., 1986. A Chemical Classification of Volcanic Rocks Based on the Total Alkali-Silica Diagram. Journal of Petrology, 27(3), 745-750. DOI: https://doi.org/10.1093/petrology/27.3.745

Lukács, R., Harangi, Sz., Guillong, M., Bachmann, O., Fodor, L., Buret, Y., Dunkl, I., Sliwinski, J., von Quadt, A., Peytcheva, I., Zimmerer, M., 2018. Early to Mid-Miocene syn extensional massive silicic volcanism in the Pannonian Basin (East-Central Europe): Eruption chronology, correlation potential and geodynamic implications. Earth-Science Reviews, 179, 1-19. DOI: https://doi.org/10.1016/j.earscirev.2018.02.005

Márton, E., 2007. Correlation of Miocene Volcanics in the Area of the North Hungary Paleogene Basin by the Combination of Palaeomagnetic Marker Horizons and Magnetic Polarities. Joannea Geologie & Paläontologie, 9, 63-65.

Márton, E., Vass, D., Túnyi, I., Márton, P., Zelenka, T., 2007. Paleomagnetic properties of the ignimbrites from the famous fossil footprints site, Ipolytarnóc (close to the Hungarian-Slovak frontier) and their age assignment. Geologica Carphatica, 58(6), 531-540.

Miall, A.D., 2006. The geology of fluvial deposits. New York, Springer, 582pp.

Nagy, E., 2005. Palynological evidence for Neogene climatic change in Hungary. Budapest, Ocassional Papers of the Geological Institute of Hungary, 205, 120pp.

Nagymarosy, A., Müller, P., 1988. Biostratigraphical aspects of the Neogene in the Pannonian Basin. In: Royden, L.H., Horváth, F. (eds.). The Pannonian Basin: A Study in Basin Evolution. American Association of Petroleum Geologists Memoir, 45, 69-77.

Němejc, F., 1963. Výsledky paleofloristických výskumú voblasti Modrého Kamene a Šahú na Jižním Slovensku. Geologické práce, Správy, 27, 115-119.

Němejc, F., Knobloch, E., 1969. Spodnomiocenní kvetena z Lipovan u Lučence. Geologické práce, Správy, 50, 204-206.

Němejc, F., Knobloch, E., 1973. Die Makroflora der Salgótarjáner Schichtengruppe (Die Flora aus Lipovany). In: Papp, A., Rögl, F., Seneš, J. (eds.). Cronostratigraphie und Neostratotypen, Miozän der zentralen Paratethys; M_2 Ottnangien. Bratislava, Slovak Academy of Sciences, 694-759.

Németh, K., Martin, U., 2007. Practical Volcanology, Lecture Notes for Understanding Volcanic Rocks from Field Based Studies. Budapest, Geological Institue of Hungary, 221pp.

Nováková, P., Rybár, S., Šarinová, K., Nagy, A., Hudáčková, N., Jamrich, M., Teodoridis, V., Kováčová, M., Šujan, M., Vlček, T., Kováč, M., 2020. The late Badenian-Sarmatian (Serravallian) environmental transition calibrated by sequence stratigraphy (Eastern Danube Basin, Central Paratethys). Geologica Carpathica, 71(4), 291-313. DOI: https://doi.org/10.31577/GeolCarp.71.4.1

Pálfy, J., Mundil, R., Renne, P.R., Bernor, R.L., Kordos, L., Gasparik, M., 2007. U–Pb and $^{40}Ar/^{39}Ar$ dating of the Miocene fossil track site at Ipolytarnóc (Hungary) and its implications. Earth and Planetary Science Letters, 258, 160-174. DOI: https://doi.org/10.1016/j.epsl.2007.03.029

Pearce, J.A., 1996. A User´s Guide to Basalt Discrimination Diagrams. In: Wyman, D.A. (ed.). Trave Element Geochemistry of Volcanic Rocks: Applications for Massive Sulphide Exploration. Geological Association of Canada, 12, 79-113.

Peccerillo, A., Taylor, S.R., 1976. Geochemistry of Eocene Calc-Alkaline Volcanic Rocks from the Kastamonu Area, Northern Turkey. Contributions to Mineralogy and Petrology, 58, 63-81. DOI: https://doi.org/10.1007/BF00384745

Renne, P.R., Mundil, R., Balco, G., Min, K., Ludwig, K.R., 2010. Joint determination of 40K decay constants and 40Ar*/40K for the Fish Canyon sanidine standard, and improved accuracy for $^{40}Ar/^{39}Ar$ geochronology. Geochimica et Cosmochimica Acta, 75(17), 5097-5100. DOI: https://doi.org/10.1016/j.gca.2010.06.017

Renne, P.R., Balco, G., Ludwig, K.R., Mundil, R., Min, K., 2011. Response to the comment by Schwarz *et al.*, on “Joint determination of 40K decay constants and 40Ar*/40K for the Fish Canyon sanidine standard, and improved accuracy for $^{40}Ar/^{39}Ar$ geochronology” by Renne *et al.*, 2010. Geochimica et Cosmochimica Acta, 74, 5349-5367. DOI: https://doi.org/10.1016/j.gca.2011.06.021

Renne, P.R., Deino, A.L, Hilgen, F.J., Kuiper, K.F., Mark, D.F., Mitchell, W.S., Morgan, L.E., Mundil, R., Smit, J., 2013. Time scales of critical events around the Cretaceous-Paleogene boundary. Science, 339(6120), 684-687. DOI: https://doi.org/10.1126/science.1230492

Repčok, I., 1987. Vek niektorých vulkanitov Krupinskej planiny, Burdy a Cerovej vrchoviny metódou stôp po štiepení uránu. Geologické práce, Správy, 86, 173-177.

Rieder, M., Cavazzini, G., D‘yakonov, Y., Frank-Kamenetskii, V.A., Gottardi, G., Guggenheim, S., Koval, P.V., Müller, G., Neiva, A.M.R., Radoslovich, E.W., Robert, J.-L., Sassi, F.P., Takeda, H., Weiss, Z., Wones, D.R., 1998. Nomenclature of the Micas. The Canadian Mineralogist, 36, 586-595. DOI: https://doi.org/10.1180/002646199548385

Roetzel, R., de Leeuw, A., Mandic, O., Márton, E., Nehyba, S., Kuiper, K., Scholger, R., Wimmer-Frey, I., 2014. Lower Miocene (upper Burdigalian, Karpatian) volcanic ash fall at the south-eastern margin of the Bohemian Massif in Austria – New evidence from Ar/Ar-dating, palaeomagnetic, geochemical and mineralogical investigations. Austrian Journal of Earth Sciences, 107(2), 2-22.

Ruman, A., Ćorić, S., Halásová, E., Harzhauser, M., Hudáčková, N., Jamrich, M., Palzer-Khomenko, M., Kranner, M., Mandic, O., Rybár, S., Šimo, V., Šujan, M., Kováč, M., 2021. The “Rzehakia beds” on the northern shelf of the Pannonian Basin: biostratigraphic and palaeoenvironmental implications. Facies, 67(1). DOI: https://doi.org/10.1007/s10347-020-00609-6

Schaltegger, U., Davies, J.H., 2017. Petrochronology of zircon and baddeleyite in igneous rocks: Reconstructing magmatic processes at high temporal resolution. Reviews in Mineralogy and Geochemistry, 83, 297-328. DOI: https://doi.org/10.2138/rmg.2017.83.10

Sitár, V., Kvaček, Z., 1997. Additions and revisions to the early Miocene flora of Lipovany (Southern Slovakia). Geologica Carpathica, 48(4), 263-280.

Sun, S.-s., McDonough, W.F., 1989. Chemical and isotopic systematics of oceanic basalts: implications for mantle composition and processes. London, Geological Society, 42, 313-345. DOI: https://doi.org/10.1144/GSL.SP.1989.042.01.19

TimeScale Creator GT, 2016. The age model is from: Ogg, J.G., Ogg, G.M., Gradstein, F.M., 2016. A Concise Geologic Time Scale. Elsevier, 240pp. Downloaded: August 2020. Website: https://timescalecreator.org/index/index.php Tischendorf, G., Förster, H.-J., Gottesmann, B., Rieder, M., 2007. True and brittle micas: composition and solid-solution series. Mineralogical Magazine, 71(3), 285-320. DOI: https://doi.org/10.1180/minmag.2007.071.3.285

Vass, D., Elečko, M., Kantorová, V., Lehotayová, R., Klubert, J., 1987. Prvý nález morského otnangu v juhoslovenskej panve. Mineralia Slovaca, 19(5), 417-422.

Vass, D., Elečko, M. (eds.), Bezák, V., Bodnár, J., Pristaš, J., Konečný, V., Lexa, J., Molák, B., Straka, P., Stankovič, J., Stolár, M., Škvarka, L., Vozár, M., Vozárová, A., 1992. Vysvetlivky ku geologickej mape Lučenskej kotliny a Cerovej vrchoviny 1:50 000. Bratislava, Geologický ústav Dionýza Štúra, 196pp.

Vass, D. (ed.), Bezák, V., Elečko, M., Konečný, V., Lexa, J., Pristaš, J., Straka, P., Vozár, J., 1992. Geological Map of the Lučenská kotlina Depression and Cerová vrchovina Upland. In: Geologická mapa Slovenska M 1:50 000. Bratislava, Štátny geologický ústav Dionýza Štúra, 2013. Website: http://apl.geology.sk/gm50js. Last access: August 2020.

Vass, D., 2002. Lithostratigraphy of Western Carpathians: Neogene and Buda Paleogene. Bratislava, State Geological Institute of Dionýz Štúr, 200pp.

Vass, D., Kráľ, J., Fordinál, K., Elečko, M., 2003. Hodnotenie výsledkov stronciovej izotopovej stratigrafie juhoslovenského kenozoika. Mineralia Slovaca, 35, 117-124.

Vass, D., Túnyi, I., Márton, E., 2006. The Feher hegy Formation: Felsitic ignimbrites and tuffs at Ipolytarnoc (Hungary), their age and position in Lower Miocene of Northern Hungary and Southern Slovakia. Slovak Geological Magazine, 12(2), 139-145.

Verati, C., Jourdan, F., 2014. Modelling effect of sericitization of plagioclase on the $^{40}K/^{40}Ar$ and $^{40}Ar/^{39}Ar$ chronometers: Implication for dating basaltic rocks and mineral deposits. London, Geological Society, 378(1), 155-174. DOI: https://doi.org/10.1144/SP378.14

Manuscript received September 2020;
revision accepted March 2021;
published Online May 2021.

APPENDIX I

Lipovany plagioclase

Relative Abundances			^{36}Ar [V]	%1σ	^{37}Ar [V]	%1σ	^{38}Ar [V]	%1σ	^{39}Ar [V]	%1σ	^{40}Ar [V]	%1σ	$^{40}(r)/^{39}(k)$ ± 2σ	Age ± 2σ (Ma)	$^{40}Ar(r)$ (%)	$^{39}Ar(k)$ (%)	K/Ca ± 2σ
0M60304	15,00%	4	0,0000123	5,657	0,0018744	57,21	0,0000198	182,223	0,0000725	12,677	0,0043152	0,778	11,05603 ± 6,99025	16,27 ± 10,24	18,25	1,22	0,02 ± 0,023
0M60284	15,00%	4	0,0000075	10,999	0,0027239	29,216	0,0000457	78,614	0,0005496	1,363	0,0083151	0,421	11,50065 ± 0,98572	16,92 ± 1,44	75,76	9,41	0,105 ± 0,061
0M60290	15,00%	4	0,0000054	11,4	0,0022892	41,222	0,0000356	113,862	0,0004702	2,099	0,0068541	0,51	11,5875 ± 0,98744	17,04 ± 1,45	79,23	8,05	0,106 ± 0,088
0M60306	15,00%	4	0,0000138	3,965	0,0018109	65,531	0,000013	260,38	0,0003451	2,586	0,007959	0,453	11,60085 ± 1,26837	17,06 ± 1,86	50,11	5,91	0,099 ± 0,129
0M60288	15,00%	4	0,0000036	17,169	0,0042288	25,361	0,0000389	83,462	0,0003588	2,839	0,0049145	0,687	11,74548 ± 1,33768	17,27 ± 1,96	85,05	6,11	0,044 ± 0,022
0M60300	15,00%	4	0,0000071	8,592	0,0003866	226,11	0,0000771	46,13	0,0000316	36,328	0,0024314	1,471	11,36491 ± 15,08671	16,72 ± 22,09	14,65	0,54	0,042 ± 0,193
0M60292	15,00%	4	0,0000069	9,734	0,0024364	41,007	0,0000024	1739,765	0,0003371	3,124	0,0058882	0,628	11,978 ± 1,50750	17,62 ± 2,21	68,23	5,76	0,072 ± 0,059
0M60296	15,00%	4	0,0000251	2,554	0,0060404	22,569	0,0000324	120,543	0,000739	1,27	0,0159343	0,259	12,14031 ± 0,68406	17,85 ± 1,00	55,98	12,62	0,063 ± 0,029
0M60270	15,00%	4	0,0000124	4,444	0,0034298	16,216	0,0000247	202,363	0,0005399	2,188	0,009988	0,248	12,20396 ± 0,83564	17,95 ± 1,22	65,68	9,23	0,082 ± 0,027
0M60286	15,00%		0,0000157	3,344	0,0019616	59,861	0,0000946	40,25	0,0004837	2,381	0,0107619	0,34	12,92691 ± 0,98816	19 ± 1,45	57,93	8,28	0,128 ± 0,153
0M60294	15,00%		0,0000203	3,397	0,0071345	13,11	0,0000151	256,009	0,0004272	2,724	0,0112265	0,318	13,60691 ± 1,28988	20 ± 1,89	51,18	7,25	0,031 ± 0,008
0M60282	15,00%		0,0000249	2,207	0,0054588	16,602	0,0000637	63,502	0,0009277	0,774	0,0198989	0,185	13,94853 ± 0,45241	20,5 ± 0,66	64,76	15,87	0,088 ± 0,029
0M60302	15,00%		0,000009	6,629	0,0007744	121,124	0,0000015	2231,178	0,0001366	6,376	0,0045862	0,839	14,38412 ± 3,43394	21,13 ± 5,02	42,68	2,34	0,091 ± 0,222
0M60308	15,00%		0,0000028	21,265	0,0013232	69,902	0,000017	199,42	0,0001135	10,241	0,0024432	1,749	15,15849 ± 4,71614	22,26 ± 6,88	69,84	1,93	0,044 ± 0,063
0M60298	15,00%		0,0000108	5,443	0,0016271	64,143	0,0000387	124,407	0,0003193	2,663	0,011449	0,323	26,26898 ± 1,87765	38,41 ± 2,72	73	5,47	0,102 ± 0,131
		Σ	0,0001775	1,364	0,0435	8,922	0,0000199	758,308	0,0058518	0,661	0,1269655	0,11					

Information on Analysis and Constants Used in Calculations	
Sample = LIPOVANY-PLG	Age Equations = Min et al. (2000)
Material = plagioclase	Negative Intensities = Allowed
Location = Laser	Decay Constant 40K = 5.531 ± 0.013 E-10 1/a
Analyst = Adam Frew	Decay Constant 39Ar = 2.940 ± 0.029 E-07 1/h
Project = NEOGENE TUFF_RYBAR_2020	Decay Constant 37Ar = 8.264 ± 0.009 E-04 1/h
Mass Discrimination Law = POW	Decay Constant 36Cl = 2.303 ± 0.046 E-06 1/a
Irradiation = I28t3h	Decay Constant 40K(EC,β⁺) = 0.576 ± 0.002 E-10 1/a
J = 0.00081730 ± 0.00000033	Decay Constant 40K(β⁻) = 4.955 ± 0.013 E-10 1/a
FCs = 28.294 ± 0.037 Ma	Atmospheric Ratio 40/36(a) = 298.56 ± 0.30
IGSN = Undefined	Atmospheric Ratio 38/36(a) = 0.1869 ± 0.0002
Preferred Age = Undefined	Production Ratio 39/37(ca) = 0.000695 ± 0.000009
Classification = Undefined	Production Ratio 38/37(ca) = 0.000020 ± 0.000001
Experiment Type = Undefined	Production Ratio 36/37(ca) = 0.000265 ± 0.000002
Extraction Method = Undefined	Production Ratio 40/39(k) = 0.000702 ± 0.000087
Heating = 60 sec	Production Ratio 38/39(k) = 0.012150 ± 0.000030
Isolation = 3.00 min	Production Ratio 36/38(cl) = 263.00 ± 13.15
Instrument = ARGUS VI	Scaling Ratio K/Ca = 0.520
Lithology = Undefined	Abundance Ratio 40K/K = 1.1700 ± 0.0100 E-04
Lat-Lon = Undefined - Undefined	Atomic Weight K = 39.0983 ± 0.0001 g
Feature = Undefined	

Results	$^{40}(a)/^{36}(a)$ ± 2σ	$^{40}(r)/^{39}(k)$ ± 2σ	Age ± 2σ (Ma)	MSWD	$^{39}Ar(k)$ (%,n)	K/Ca ± 2σ
Age Plateau		11,89446 ± 0,37090	17,49 ± 0,54	0,3	58,86	0,053 ± 0,018
		± 3,12%	± 3,10%	96%	9	
			Full External Error ± 0,56	2	2σ Confidence Limit	
			Analytical Error ± 0,54	1	Error Magnification	
Total Fusion Age		13,30023 ± 0,32640	19,55 ± 0,48		15	0,07 ± 0,012
		± 2,45%	± 2,44%			
			Full External Error ± 0,50			
			Analytical Error ± 0,48			
Normal Isochron	305,43 ± 27,09	11,71936 ± 0,70279	17,24 ± 1,03	0,32	58,86	
	± 8,87%	± 6,00%	± 5,97%	94%	9	
			Full External Error ± 1,04	2,07	2σ Confidence Limit	
			Analytical Error ± 1,03	1	Error Magnification	
				37	Number of Iterations	
				0,000113756	Convergence	
Inverse Isochron	305,23 ± 27,77	11,75119 ± 0,72414	17,28 ± 1,06	0,31	58,86	
	± 9,10%	± 6,16%	± 6,13%	95%	9	
			Full External Error ± 1,07	2,07	2σ Confidence Limit	
			Analytical Error ± 1,06	1	Error Magnification	
				3	Number of Iterations	
				7,23035E-05	Convergence	
				70%	Spreading Factor	

Lipovany biotite

Relative Abundances			^{36}Ar [V]	%1σ	^{37}Ar [V]	%1σ	^{38}Ar [V]	%1σ	^{39}Ar [V]	%1σ	^{40}Ar [V]	%1σ	^{40}(r)/^{39}(k) ±2σ	Age ±2σ (Ma)	^{40}Ar(r) (%)	^{39}Ar(k) (%)	K/Ca ±2σ
0M61245	15,00%		0,0009279	0,341	0,0003289	510,756	0,0001773	31,194	0,0015402	0,857	0,2723815	0,065	3,01168 ± 1,31080	4,46 ± 1,94	1,7	1,73	2,43 ± 24,87
0M61240	15,00%		0,0008251	0,265	0,0001598	1180,738	0,0001706	30,186	0,0012443	0,984	0,2431495	0,074	2,54998 ± 1,18360	3,77 ± 1,75	1,3	1,4	4,05 ± 95,64
0M61247	15,00%		0,0008094	0,303	0,0003012	665,704	0,0002166	24,377	0,0017143	0,524	0,2400054	0,075	0,95059 ± 0,94168	1,41 ± 1,39	0,68	1,93	2,96 ± 39,39
0M61248	15,00%		0,0001078	1,212	0,00134	145,803	0,0000265	201,719	0,0002239	5,31	0,0323428	0,542	1,14938 ± 4,09285	1,7 ± 6,04	0,79	0,25	0,09 ± 0,25
0M61253	15,00%		0,0009684	0,312	0,0035715	55,911	0,0002801	13,384	0,0053918	0,265	0,3305222	0,017	7,73563 ± 0,35911	11,4 ± 0,53	12,61	6,06	0,78 ± 0,88
0M61251	15,00%		0,0012144	0,268	0,0055644	39,006	0,0004345	8,331	0,0071861	0,154	0,4180709	0,015	7,79126 ± 0,29382	11,48 ± 0,43	13,39	8,08	0,67 ± 0,52
0M61239	15,00%		0,0017186	0,225	0,0012648	182,926	0,0004862	7,357	0,0097976	0,106	0,5912247	0,011	7,98372 ± 0,26190	11,76 ± 0,38	13,23	11,02	4,03 ± 14,74
0M61237	15,00%		0,0007378	0,331	0,0002355	1004,035	0,0002988	11,923	0,0097929	0,173	0,3175548	0,018	9,9297 ± 0,16439	14,61 ± 0,24	30,62	11,02	21,62 ± 434,23
0M61249	15,00%		0,0002809	0,426	0,0000316	5592,602	0,0002293	15,664	0,0100519	0,139	0,196618	0,027	11,21512 ± 0,08491	16,5 ± 0,12	57,34	11,31	165,43 ± 18503,50
0M61244	15,00%	4	0,0000492	1,322	0,0034079	49,436	0,0000713	55,969	0,002702	0,315	0,0464451	0,1	11,63898 ± 0,19278	17,12 ± 0,28	67,77	3,04	0,41 ± 0,41
0M61236	15,00%	4	0,0000427	1,879	0,0015104	142,864	0,0000584	65,112	0,0047849	0,169	0,0686166	0,081	11,70096 ± 0,13165	17,21 ± 0,19	81,58	5,38	1,65 ± 4,71
0M61241	15,00%	4	0,0000382	1,832	0,0005291	357,932	0,0002822	12,211	0,0157923	0,105	0,1964814	0,025	11,72229 ± 0,04133	17,24 ± 0,06	94,22	17,77	15,52 ± 111,11
0M61243	15,00%	4	0,0000271	2,568	0,0002283	900,648	0,0001672	26,657	0,0108262	0,092	0,1357362	0,039	11,78818 ± 0,05437	17,34 ± 0,08	94,02	12,18	24,66 ± 444,18
0M61235	15,00%	4	0,0000402	1,523	0,0037478	52,723	0,0000866	34,206	0,0041616	0,267	0,0608829	0,088	11,82157 ± 0,13474	17,39 ± 0,20	80,75	4,68	0,58 ± 0,61
0M61252	15,00%	4	0,0000119	6,013	0,0011523	169,982	0,0000486	86,603	0,0036805	0,333	0,0471573	0,109	11,87021 ± 0,16673	17,46 ± 0,24	92,62	4,14	1,66 ± 5,65
		Σ	0,0077999	0,105	0,0155669	49,773	0,0030344	5,393	0,0888906	0,053	3,1971894	0,013					

Information on Analysis and Constants Used in Calculations	
Sample = LIPOVANY-BIO	Age Equations = Min et al. (2000)
Material = biotite	Negative Intensities = Allowed
Location = Laser	Decay Constant 40K = 5.531 ± 0.013 E-10 1/a
Analyst = Adam Frew	Decay Constant 39Ar = 2.940 ± 0.029 E-07 1/h
Project = NEOGENE TUFF_RYBAR_2020	Decay Constant 37Ar = 8.264 ± 0.009 E-04 1/h
Mass Discrimination Law = POW	Decay Constant 36Cl = 2.303 ± 0.046 E-06 1/a
Irradiation = I28t3h	Decay Constant 40K(EC,β⁺) = 0.576 ± 0.002 E-10 1/a
J = 0.00081730 ± 0.00000033	Decay Constant 40K(β⁻) = 4.955 ± 0.013 E-10 1/a
FCs = 28.294 ± 0.037 Ma	Atmospheric Ratio 40/36(a) = 298.56 ± 0.30
IGSN = Undefined	Atmospheric Ratio 38/36(a) = 0.1869 ± 0.0002
Preferred Age = Undefined	Production Ratio 39/37(ca) = 0.000695 ± 0.000009
Classification = Undefined	Production Ratio 38/37(ca) = 0.000020 ± 0.000001
Experiment Type = Undefined	Production Ratio 36/37(ca) = 0.000265 ± 0.000002
Extraction Method = Undefined	Production Ratio 40/39(k) = 0.000702 ± 0.000087
Heating = 60 sec	Production Ratio 38/39(k) = 0.012150 ± 0.000030
Isolation = 3.00 min	Production Ratio 36/38(cl) = 263.00 ± 13.15
Instrument = ARGUS VI	Scaling Ratio K/Ca = 0.520
Lithology = Undefined	Abundance Ratio 40K/K = 1.1700 ± 0.0100 E-04
Lat-Lon = Undefined - Undefined	Atomic Weight K = 39.0983 ± 0.0001 g
Feature = Undefined	

Results	^{40}(a)/^{36}(a) ±2σ	^{40}(r)/^{39}(k) ±2σ	Age ±2σ (Ma)	MSWD	^{39}Ar(k) (%,n)	K/Ca ±2σ
Age Plateau		11,74922 ± 0,04014 ± 0,34%	17,28 ± 0,06 ± 0,35%	1,77	47,19	0,09 ± 0,44
				11%	6	
			Full External Error ± 0,14	2,26	2σ Confidence Limit	
			Analytical Error ± 0,06	1,331	Error Magnification	
Total Fusion Age		9,78504 ± 0,06164 ± 0,63%	14,4 ± 0,09 ± 0,63%		15	2,97 ± 2,96
			Full External Error ± 0,14			
			Analytical Error ± 0,09			
Normal Isochron	293,22 ± 14,00 ± 4,78%	11,77175 ± 0,06592 ± 0,56%	17,31 ± 0,10 ± 0,56%	2,17	47,19	
				7%	6	
			Full External Error ± 0,16	2,41	2σ Confidence Limit	
			Analytical Error ± 0,10	1,4715	Error Magnification	
				75	Number of Iterations	
				0,000117603	Convergence	
Inverse Isochron	295,93 ± 14,06 ± 4,75%	11,7587 ± 0,06646 ± 0,57%	17,29 ± 0,10 ± 0,57%	2,15	47,19	
				7%	6	
			Full External Error ± 0,16	2,41	2σ Confidence Limit	
			Analytical Error ± 0,10	1,4651	Error Magnification	
				3	Number of Iterations	
				4,8163E-06	Convergence	
				26%	Spreading Factor	

Mučín plagioclase

Relative Abundances			^{36}Ar [V]	%1σ	^{37}Ar [V]	%1σ	^{38}Ar [V]	%1σ	^{39}Ar [V]	%1σ	^{40}Ar [V]	%1σ	^{40}(r)/^{39}(k) ± 2σ	Age ± 2σ (Ma)	^{40}Ar(r) (%)	^{39}Ar(k) (%)	K/Ca ± 2σ
0M61100	16,00%		0,0000062	10,799	0,001175	136,343	0,0000398	116,315	0,0000422	25,892	0,0015974	5,837	3,8098 ± 12,47000	5,64 ± 18,49	9,87	1,88	0,018 ± 0,051
0M61095	16,00%		0,0000033	21,331	0,0032896	51,653	0,000006	609,669	0,0000512	18,329	0,0010948	8,654	2,85848 ± 10,05313	4,23 ± 14,89	13,96	2,43	0,008 ± 0,009
0M61096	16,00%		0,0000019	34,092	0,0013197	129,301	0,0000489	85,928	0,000028	29,394	0,0006093	15,389	1,73514 ± 17,46135	2,57 ± 25,84	8,23	1,31	0,011 ± 0,030
0M61097	16,00%		0,0000065	9,912	0,0013804	122,89	0,0000421	82,053	0,0000344	23,635	0,0019876	4,71	1,85435 ± 14,36143	2,74 ± 21,26	3,3	1,61	0,013 ± 0,033
0M61112	16,00%		0,0000028	20,59	0,0017181	99,172	0,0000705	73,238	0,0000431	22,127	0,0011577	7,967	4,50899 ± 10,80398	6,65 ± 15,91	17,25	2,01	0,013 ± 0,027
0M61104	16,00%		0,0000038	14,17	0,004514	31,886	0,0000089	381,568	0,0000696	15,872	0,0011827	7,792	6,07397 ± 6,85750	8,95 ± 10,08	34,15	3,02	0,008 ± 0,006
0M61099	16,00%	4	0,0000047	13,836	0,0010235	197,452	0,0000484	82,054	0,000269	3,974	0,0039721	2,344	9,83908 ± 2,16042	14,48 ± 3,17	66,46	12,2	0,136 ± 0,538
0M61113	16,00%	4	0,0000099	7,018	0,0006458	278,877	0,0000173	215,886	0,0002694	4,478	0,0056224	1,646	10,10931 ± 2,19287	14,88 ± 3,21	48,36	12,23	0,217 ± 1,208
0M61101	16,00%	4	0,0000096	5,861	0,0006053	287,977	0,0000045	768,275	0,0002403	5,065	0,0053959	1,718	10,34903 ± 2,22475	15,23 ± 3,26	46,16	10,94	0,207 ± 1,191
0M61105	16,00%	4	0,0000067	9,632	0,0014153	146,387	0,0000252	155,889	0,0001087	7,922	0,0030445	3,028	10,67868 ± 5,30335	15,71 ± 7,77	37,77	4,9	0,04 ± 0,116
0M61111	16,00%	4	0,0000013	48,511	0,0008283	193,153	0,0000212	236,148	0,0002195	3,438	0,0028447	3,36	11,48424 ± 2,41989	16,89 ± 3,54	88,37	9,95	0,137 ± 0,531
0M61103	16,00%	4	0,0000112	8,696	0,0046671	41,949	0,0000171	241,208	0,0003247	2,86	0,0067543	1,419	11,78328 ± 2,23991	17,33 ± 3,28	56,08	14,62	0,036 ± 0,030
0M61109	16,00%	4	0,0000013	54,742	0,0000388	4490,877	0,0000176	200,082	0,0000941	10,706	0,0015147	6,212	11,94523 ± 6,34727	17,57 ± 9,29	74,17	4,28	1,261 ± 113,242
0M61108	16,00%	4	0,0000133	4,353	0,0030653	53,913	0,0000303	127,039	0,0001807	5,322	0,0058829	1,598	12,10637 ± 2,95117	17,8 ± 4,32	36,76	8,12	0,03 ± 0,033
0M61107	16,00%	4	0,0000085	8,257	0,0013856	133,816	0,000048	93,689	0,0002318	3,875	0,0057226	1,621	14,22957 ± 2,61422	20,91 ± 3,82	57,4	10,5	0,087 ± 0,232
		Σ	0,0000911	2,854	0,0104457	65,262	0,0001129	139,684	0,0022066	1,728	0,0483835	0,749					

Information on Analysis and Constants Used in Calculations

Sample = MUCIN-PLG	Age Equations = Min et al. (2000)
Material = plagioclase	Negative Intensities = Allowed
Location = Laser	Decay Constant 40K = 5.531 ± 0.013 E-10 1/a
Analyst = Adam Frew	Decay Constant 39Ar = 2.940 ± 0.029 E-07 1/h
Project = NEOGENE TUFF_RYBAR_2020	Decay Constant 37Ar = 8.264 ± 0.009 E-04 1/h
Mass Discrimination Law = POW	Decay Constant 36Cl = 2.303 ± 0.046 E-06 1/a
Irradiation = I28t3h	Decay Constant 40K(EC,β⁺) = 0.576 ± 0.002 E-10 1/a
J = 0.00081730 ± 0.00000033	Decay Constant 40K(β⁻) = 4.955 ± 0.013 E-10 1/a
FCs = 28.294 ± 0.037 Ma	Atmospheric Ratio 40/36(a) = 298.56 ± 0.30
IGSN = Undefined	Atmospheric Ratio 38/36(a) = 0.1869 ± 0.0002
Preferred Age = Undefined	Production Ratio 39/37(ca) = 0.000695 ± 0.000009
Classification = Undefined	Production Ratio 38/37(ca) = 0.000020 ± 0.000001
Experiment Type = Undefined	Production Ratio 36/37(ca) = 0.000265 ± 0.000002
Extraction Method = Undefined	Production Ratio 40/39(k) = 0.000702 ± 0.000087
Heating = 60 sec	Production Ratio 38/39(k) = 0.012150 ± 0.000030
Isolation = 3.00 min	Production Ratio 36/38(cl) = 263.00 ± 13.15
Instrument = ARGUS VI	Scaling Ratio K/Ca = 0.520
Lithology = Undefined	Abundance Ratio 40K/K = 1.1700 ± 0.0100 E-04
Lat-Lon = Undefined - Undefined	Atomic Weight K = 39.0983 ± 0.0001 g
Feature = Undefined	

Results	^{40}(a)/^{36}(a) ± 2σ	^{40}(r)/^{39}(k) ± 2σ	Age ± 2σ (Ma)	MSWD	^{39}Ar(k) (%,n)	K/Ca ± 2σ
Age Plateau		11,21656 ± 0,94144 ± 8,39%	16,5 ± 1,38 ± 8,36%	1,17 32%	87,73 9	0,034 ± 0,022
			Full External Error ± 1,38	2	2σ Confidence Limit	
			Analytical Error ± 1,38	1,0799	Error Magnification	
Total Fusion Age		10,02556 ± 0,98470 ± 9,82%	14,76 ± 1,44 ± 9,78%		15	0,109 ± 0,143
			Full External Error ± 1,45			
			Analytical Error ± 1,44			
Normal Isochron	337,02 ± 61,87 ± 18,36%	9,53277 ± 2,38731 ± 25,04%	14,03 ± 3,50 ± 24,95%	0,91 50%	87,73 9	
			Full External Error ± 3,50	2,07	2σ Confidence Limit	
			Analytical Error ± 3,50	1	Error Magnification	
				59	Number of Iterations	
				8,86159E-05	Convergence	
Inverse Isochron	324,7 ± 59,48 ± 18,32%	10,46058 ± 2,00470 ± 19,16%	15,39 ± 2,94 ± 19,08%	1,23 28%	87,73 9	
			Full External Error ± 2,94	2,07	2σ Confidence Limit	
			Analytical Error ± 2,94	1,1101	Error Magnification	
				4	Number of Iterations	
				2,55547E-05	Convergence	
				49%	Spreading Factor	

APPENDIX II

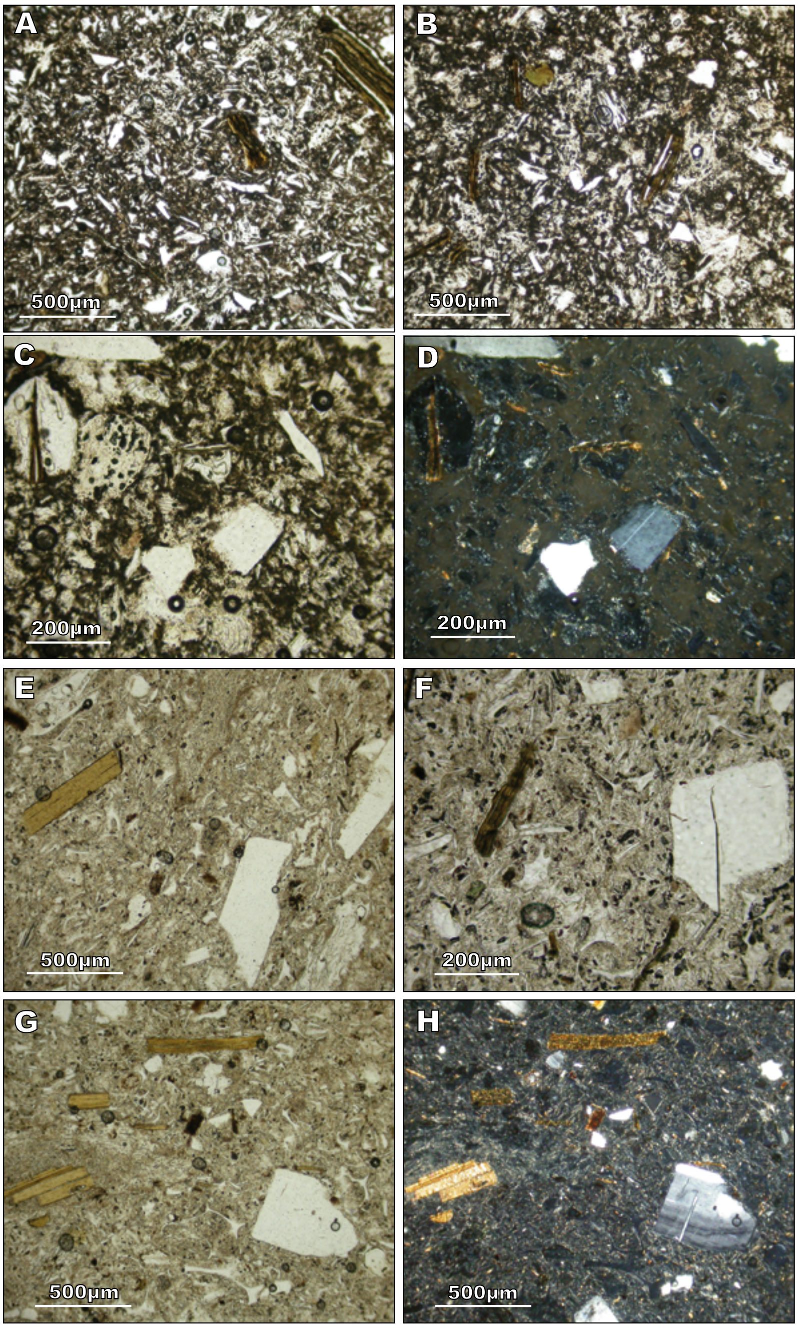

FIGURE I. Microphotographs of dated samples. Mučín fine tuff (Ft) with crystalloclasts of altered biotite, plagioclase, quartz, glass shards and pumice fragments (A-C plane polarized light; D-crossed nicols). Lipovany lapilli tuff (Lt) with crystalloclasts of altered biotite, plagioclase, quartz, glass shards and pumice fragments (E-F plane polarized light; Hcrossednicols).